Dalton Transactions

PAPER

View Article Online
View Journal | View Issue

Cite this: *Dalton Trans.*, 2015, **44**, 12598

Two types of novel tetra-iron substituted sandwich-type arsenotungastates with supporting lanthanide pendants†

Lijuan Chen, Fang Zhang, Xing Ma, Jie Luo* and Junwei Zhao*

Two classes of novel tetra-iron substituted sandwich-type arsenotungastates (ATs) with supporting lanthanide (Ln) pendants KNa_2 $[Ln(H_2O)_7][Fe_4(H_2O)_{10}(B\text{-}\beta\text{-}AsW_9O_{33})_2]\cdot 21H_2O$ [Ln = La^{III} (**1**), Pr^{III} (**2**), Nd^{III} (**3**), Sm^{III} (**4**)] and $[Ln(H_2O)_8]_2[Fe_4(H_2O)_8(L\text{-thr})_2(B\text{-}\beta\text{-}AsW_9O_{33})_2]\cdot 20H_2O$ [Ln = La^{III} (**5**), Pr^{III} (**6**), Nd^{III} (**7**), Sm^{III} (**8**), Eu^{III} (**9**), Gd^{III} (**10**), Tb^{III} (**11**), Dy^{III} (**12**), Er^{III} (**13**)] (L-thr = L-threonine) have been synthesized by the hydrothermal reaction of the $[As_2W_{19}O_{67}(H_2O)]^{14-}$ precursor with Fe^{3+} cations and Ln^{3+} cations in the presence of L-thr or L-leucine and L-alanine, and further characterized by elemental analyses, IR spectra and single-crystal X-ray diffraction. Structural analyses indicate that **1–4** display the inorganic 2-D sheet architecture constructed from tetra-iron sandwiched AT $[Fe_4(H_2O)_{10}(B\text{-}\beta\text{-}AsW_9O_{33})_2]^{6-}$ fragments by bridging $[Ln(H_2O)_7]^{3+}$ cations whereas the molecular structures of the isostructural **5–13** consist of an organic–inorganic hybrid tetra-iron substituted sandwich-type AT $[Fe_4(H_2O)_8(L\text{-thr})_2(B\text{-}\beta\text{-}AsW_9O_{33})_2]^{6-}$ fragment and two pendant $[Ln(H_2O)_8]^{3+}$ cations. As far as we know, **1–4** represent the rare inorganic 2-D extended ATs based on transition-metal substituted sandwich-type polyoxometalate units and Ln linkers and **5–13** are the first Fe–Ln heterometallic ATs with amino acid ligands. The solid state photoluminescence (PL) measurements of **9** and **11** have been performed at room temperature. The PL emission of **9** is mainly derived from the characteristic $^5D_0 \rightarrow {}^7F_2$ (J = 4–0) transitions of the Eu^{III} cations whereas the PL behavior of **11** stems from the common contribution of the $^5D_4 \rightarrow {}^7F_J$ (J = 5–3) transitions of the Tb^{III} ions and oxygen-to-metal (O → W) charge-transfer transitions of AT segments. The thermogravimetric (TG) analyses of **1–4** and **6–12** have been investigated.

Received 16th February 2015,
Accepted 24th May 2015

DOI: 10.1039/c5dt00696a

www.rsc.org/dalton

Introduction

Although the class of polyoxometalates (POMs) has been known for about 200 years, intense and profound research on this field is still full of great challenges for synthetic chemists.[1] It is well known that the oxygen-rich surface activity of lacunary POMs recommends them to function as benign inorganic multi-dentate synthons to integrate oxophile transition-metal (TM) or Ln cations, constructing a great variety of novel TM or Ln substituted POMs with potential functionalities in various fields such as catalysis, magnetism, medicine, photochemistry and materials science.[2] Thereby, using prefabricated POM precursors to react with TM or Ln cations under different conditions has developed as the most useful assembly strategy in the design and synthesis of novel composite materials such as TM substituted POMs (TMSPs) and Ln substituted POMs (LSPs) that bear features of both the POM and TM/Ln components. In the past two decades, the wide use of this assembly strategy directly has resulted in a mass of TMSPs and LSPs with interesting structures and properties such as sandwich-type $[(\alpha\text{-}XW_9O_{33})_2M_3(H_2O)_3]^{n-}$ (n = 12, X = As^{III}, Sb^{III}, M = Cu^{II}, Zn^{II}; n = 10, X = Se^{IV}, Te^{IV}, M = Cu^{II}),[3a] crown-shaped $[K \subset \{Eu(H_2O)_2(\alpha\text{-}AsW_9O_{33})\}_6]^{35-}$ and $[Cs \subset \{Eu(H_2O)_2(\alpha\text{-}AsW_9O_{33})\}_4]^{23-}$,[3b] tetrameric $[H_{56}Fe_{28}P_8W_{48}O_{248}]^{28-}$,[3c] wheel-shaped $[Cu_{20}Cl(OH)_{24}(H_2O)_{12}(P_8W_{48}O_{184})]^{25-}$,[3d] planar $\{Mn_{19}(OH)_{12}\}^{26+}$ incorporated $[Mn_{19}(OH)_{12}(SiW_{10}O_{37})_6]^{34-}$,[3e] Ce_{16}-containing $[As_{12}Ce_{16}W_{148}O_{524}(H_2O)_{36}]^{76-}$,[3f] decameric $[Ce_{20}Ge_{10}W_{100}O_{376}(OH)_4(H_2O)_{30}]^{56-}$,[3g] gadolinium-bridged $[Gd_8As_{12}W_{124}O_{432}(H_2O)_{36}]^{60-}$,[3h] saddle-shaped $[H_{34}W_{119}Se_8Fe_2O_{420}]^{54-}$,[3i] λ-shaped $[H_4CoWO(H_2O)_3(Se_2W_{26}O_{85})(Se_2W_{30}O_{107})_2]^{40-}$,[3j] and Zr_{24}-cluster-substituted $[Zr_{24}O_{22}(OH)_{10}(H_2O)_2(W_2O_{10}H)_2(GeW_9O_{34})_4(GeW_8O_{31})_2]^{32-}$.[3k]

In the field of POM chemistry, arsenotungstates (ATs) are a crucial subclass bearing enormous variety and fascinating

Henan Key Laboratory of Polyoxometalate Chemistry, Institute of Molecular and Crystal Engineering, College of Chemistry and Chemical Engineering, Henan University, Kaifeng, Henan 475004, P. R. China. E-mail: luojie@henu.edu.cn, zhaojunwei@henu.edu.cn

†Electronic supplementary information (ESI) available: The refinement details and additional figures. CCDC 1048556–1048564. For ESI and crystallographic data in CIF or other electronic format see DOI: 10.1039/c5dt00696a

properties and have received increasing attraction in the past several decades.[4] In recent years, increasing research has been concentrated on the preparation and exploitation of novel As^{III}-containing ATs since the lone pair of electrons on the As^{III} heteroatom does not allow the closed Keggin unit to form, which leads to some unique structures such as $[Ce_2O(H_2O)_5WO(H_2O)(AsW_9O_{33})_2]_2^{16-}$,[4b] $[As_{12}Ce_{16}(H_2O)_{36}W_{148}O_{524}]^{76-}$,[4c] $[\{Sn(CH_3)_2(H_2O)_2\}_3(\beta\text{-}AsW_9O_{33})]^{3-}$,[5a] and $[H_4\{Cu_9As_6O_{15}(H_2O)_6\}(\alpha\text{-}AsW_9O_{33})_2]^{8-}$.[5b] However, investigations on the reactions of the $[As_2W_{19}O_{67}(H_2O)]^{14-}$ synthon as the starting material with TM or Ln cations remain less developed even though the $[As_2W_{19}O_{67}(H_2O)]^{14-}$ precursor was discovered by Tourné *et al.* in 1973.[6a] In 2001, the structure of $[As_2W_{19}O_{67}(H_2O)]^{14-}$ was determined by Kortz *et al.* by means of a single-crystal X-ray diffraction technique, in the meantime, it was used as the precursor to generate a chair-conformation AT $[As_6W_{65}O_{217}(H_2O)_7]^{26-}$ (Fig. 1a) by controlling the pH value of the solution of $[As_2W_{19}O_{67}(H_2O)]^{14-}$.[6b] Subsequently, bis-phenyltin-sandwiched $[(C_6H_5Sn)_2As_2W_{19}O_{67}(H_2O)]^{8-}$ (Fig. 1b),[4a] monopalladium(II)-substituted $[Na_2(H_2O)_2PdWO(H_2O)(\alpha\text{-}AsW_9O_{33})_2]^{10-}$ (Fig. 1c),[6c] and dititanium-containing $[Ti_2(OH)_2As_2W_{19}O_{67}(H_2O)]^{8-}$ (Fig. 1d)[6d] ATs were successively obtained by Kortz's group. In 2007 and 2008, Wang *et al.* respectively reported a dimeric AT decorated by 3d–4f hetero-metallic ions $\{La[As_2W_{20}CuO_{67}(H_2O)_3]\}^{3-}$ (Fig. 1e)[6e] and a novel high-nuclear $\{(W_4O_9)(H_2O)_2\}$-encapsulated AT aggregate $[\{(W_4O_9)(H_2O)_2\}\{As_2W_{19}O_{67}(H_2O)\}_2]^{22-}$ (Fig. 1f).[6f] In 2010, Kortz and co-workers addressed a mono-Y^{III}-containing derivative of 19-tungsto-2-arsenate $[Yb(H_2O)_2K(H_2O)_2As_2W_{19}O_{67}(H_2O)]^{10-}$ (Fig. 1g).[6g] In 2010–2012, Boskovic *et al.* synthesized a family of polynuclear Ln substituted ATs $[Nd_3As_4W_{41}O_{141}OH(H_2O)_{10}]^{16-}$ (Fig. 1h),[6h] $[Dy_4As_2W_{22}O_{76}(H_2O)_{19}(C_2H_5NO_2)_2]^{2-}$,[6h] $[Ln_4As_5W_{40}O_{144}(H_2O)_{10}(gly)_2]^{21-}$ (Ln = Gd^{III}, Tb^{III}, Dy^{III}, Ho^{III}, Y^{III}) (Fig. 1i),[6i] $[Tb_8(pic)_6(H_2O)_{22}(B\text{-}\beta\text{-}AsW_8O_{30})_4(WO_2(pic))_6]^{12-}$ (Fig. 1j),[6j,k] $[Eu_8(pic)_6(H_2O)_{22}(B\text{-}\beta\text{-}AsW_8O_{30})_4(WO_2(pic))_6]^{12-}$,[6k] and $[Tb_2(pic)(H_2O)_2(B\text{-}\beta\text{-}AsW_8O_{30})_2(WO_2(pic))_3]^{10-}$ (Fig. 1k)[6j,k] by controlling the pH value of the $[As_2W_{19}O_{67}(H_2O)]^{14-}$ and Ln system in the conventional aqueous solution, and deeply probed the single-molecule magnet behavior of $[Dy_4As_5W_{40}O_{144}(H_2O)_{10}(gly)_2]^{21-}$,[6i] and the sensitization of lanthanide luminescence by organic and inorganic ligands in $[Tb_8(pic)_6(H_2O)_{22}(B\text{-}\beta\text{-}AsW_8O_{30})_4(WO_2(pic))_6]^{12-}$,[6j] and $[Eu_8(pic)_6(H_2O)_{22}(B\text{-}\beta\text{-}AsW_8O_{30})_4(WO_2(pic))_6]^{12-}$.[6k] In 2014, Han *et al.* communicated an organic–inorganic AT hybrid $[Ni(phen)_3]_4[As_2W_{18}O_{60}]\{[Ni(phen)_2][H_2As_2W_{18}O_{60}]\}\cdot 12H_2O$ (Fig. 1l) by means of the hydrothermal reaction technique.[6l] However, investigations on the system containing the divacant $[As_2W_{19}O_{67}(H_2O)]^{14-}$ precursor, and TM and Ln cations are sporadic,[6e] which is of great interest to us and provides us with an excellent opportunity.

Recently, the designed synthesis and intensive exploration of novel hybrid materials through the modification of POMs by heterometal components has become an emerging field which is significant for discovering new materials with latent applications in bimetallic catalysis and magnetism as well as intriguing architectures and topologies.[7] Although some phosphotungstate, germanotungstate and silicontungstate-based TM–Ln heterometallic derivatives (TLHDs) have been reported,[8] AT-based TLHDs remain largely unexplored.[9] In 2004, the first class of AT-based TLHDs $[Ln(H_2O)_5\{Ni(H_2O)\}_2As_4W_{40}O_{140}]^{21-}$ (Ln = Y^{III}, Ce^{III}, Pr^{III}, Nd^{III}, Sm^{III}, Eu^{III}, Gd^{III}) were isolated by the reaction of $[As_4W_{40}O_{140}]^{28-}$ with Ni^{2+} and Ln^{3+} ions at pH = 4.5 by Xue *et al.*[9a] In 2007, Müller and co-workers made a sandwich-type AT-based TLHD $[((VO)_2Dy(H_2O)_4K_2(H_2O)_2Na(H_2O)_2)(\alpha\text{-}B\text{-}AsW_9O_{33})_2]^{8-}$ from the self-assembly of $Na_2WO_4\cdot 2H_2O$, As_2O_3, $VOSO_4\cdot 5H_2O$ and $DyCl_3\cdot 6H_2O$.[9b] In 2008, Wang's group synthesized cryptand-shaped $[K\subset\{FeCe(AsW_{10}O_{38})(H_2O)_2\}_3]^{14-}$ using a simple one-pot procedure.[9c] In 2012, we prepared four types of 1-D and 2-D organic–inorganic hybrids assembled by ATs and Cu^{II}–$Ln^{III/IV}$ heterometals by the hydrothermal reaction of the $[A\text{-}\alpha\text{-}AsW_9O_{34}]^{9-}$ precursor with copper and Ln cations in the presence of organoamines.[9d] In the past year, we extended our study from the As^{V}-containing system to the As^{III}-containing system and utilized $[As_2W_{19}O_{67}(H_2O)]^{14-}$ as the precursor to react with TM and Ln cations in the presence of amino acid ligands to construct novel AT-based TLHDs. This was based on the fact that this precursor can transform to $[B\text{-}\alpha\text{-}AsW_9O_{33}]^{9-}$ (Fig. 2a),[4a,6b–d] $[B\text{-}\beta\text{-}AsW_9O_{33}]^{9-}$ (Fig. 2b),[6b] $[B\text{-}\beta\text{-}AsW_8O_{30}]^{9-}$ (Fig. 2c),[6h–k] $[As_2W_{18}O_{60}]^{6-}$ (Fig. 2d),[6l] and $[As_2W_{21}O_{69}(H_2O)]^{6-}$ (Fig. 2e)[10] fragments in the reaction process and amino acid ligands have flexible carboxyl and amino coordination sites and allow various coordination modes. On the basis of these considerations, we obtained two kinds of novel tetra-Fe^{III} sandwiched ATs with supporting Ln pendants $KNa_2[Ln(H_2O)_7][Fe_4(H_2O)_{10}(B\text{-}\beta\text{-}AsW_9O_{33})_2]\cdot 21H_2O$ [Ln = La^{III} (**1**), Pr^{III} (**2**), Nd^{III} (**3**), Sm^{III} (**4**)] and $[Ln(H_2O)_8]_2[Fe_4(H_2O)_8(L\text{-}thr)_2(B\text{-}\beta\text{-}AsW_9O_{33})_2]\cdot 20H_2O$ [Ln = La^{III} (**5**), Pr^{III} (**6**), Nd^{III} (**7**), Sm^{III} (**8**), Eu^{III} (**9**), Gd^{III}

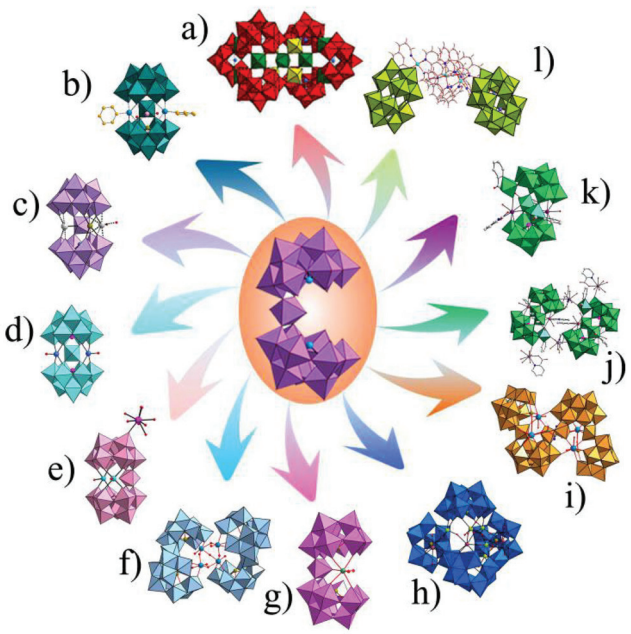

Fig. 1 The relevant ATs prepared by the $[As_2W_{19}O_{67}(H_2O)]^{14-}$ precursor.

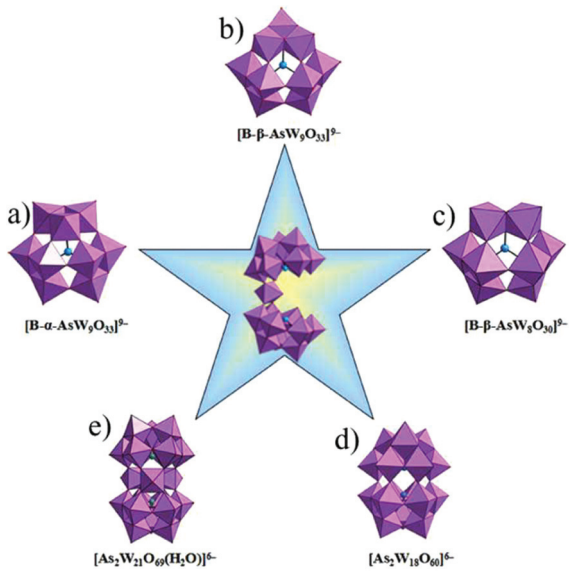

Fig. 2 The different AT fragments derived from the transformation of the $[As_2W_{19}O_{67}(H_2O)]^{14-}$ precursor.

(**10**), Tb^{III} (**11**), Dy^{III} (**12**), Er^{III} (**13**)] (L-thr = L-threonine). Notably, **1–4** stand for the scarce inorganic 2-D extended ATs based on sandwich-type TMSP units and Ln linkers while **5–13** represent the first Fe–Ln heterometallic ATs with amino acid ligands.

Experimental

Materials and physical measurements

The precursor $K_{14}[As_2W_{19}O_{67}(H_2O)]$ was synthesized according to the published procedure by Kortz *et al.*,[6b] and the purity was confirmed by IR spectroscopy. All other reagents were of at least analytical grade without further purification. C, H and N analyses were performed using a Perkin-Elmer 2400-II CHNS/O analyzer. Inductively coupled plasma atomic emission spectrometry (ICP-AES) was carried out on a Perkin-Elmer Optima 2000 ICP-AES spectrometer. IR spectra were recorded with a Nicolet 170 SXFT-IR spectrometer with a KBr pellet in the range 400–4000 cm^{-1}. TG analyses were performed under a N_2 atmosphere using a Mettler–Toledo TGA/SDTA 851^e instrument with a heating rate of 10 °C min^{-1} from 25 to 800 °C. PL and lifetime spectra were recorded using a FLS 980 Edinburgh analytical instrument furnished by a 450 W xenon lamp and a μF900H high-energy microsecond flash lamp as the excitation sources.

Preparations of 1–11

$KNa_2\{La(H_2O)_7[Fe_4(H_2O)_{10}(B\text{-}\beta\text{-}AsW_9O_{33})_2]\}\cdot 21H_2O$ (1). $K_{14}[As_2W_{19}O_{67}(H_2O)]$ (0.264 g, 0.050 mmol), $FeCl_3\cdot 6H_2O$ (0.108 g, 0.399 mmol), $LaCl_3\cdot 6H_2O$ (0.077 g, 0. 217 mmol), L-leucine (0.056 g, 0.427 mmol), L-alanine (0.046 g, 0.517 mmol) and NaCl (0.105 g, 179.7 mmol) were successively added to 7 mL of water under stirring (pH = 2.19). The resulting suspension mixture was continuously stirred for 3 h, transferred to a 25 mL Teflon-lined steel autoclave, heated at 100 °C for 5 days and then cooled to room temperature. Eventually, light yellow virgate crystals of **1** were obtained by filtering, washed with distilled water and then dried at room temperature. Yield: *ca.* 18% (based on $K_{14}[As_2W_{19}O_{67}(H_2O)]$). Anal. calcd (found %) for $H_{76}As_2Fe_4KNa_2LaO_{104}W_{18}$ (**1**): H 1.36 (1.48), Na 0.81 (0.70), K 0.69 (0.81), Fe 3.96 (3.89), La 2.46 (2.60), W 58.60 (59.51). IR (KBr, cm^{-1}): 3407 (s), 1633 (s), 1459 (m), 1395 (m), 1354 (m), 960 (s), 881 (s), 802 (vs), 662 (s), 519 (m), 479 (w), 418 (w) (Fig. S1†).

$KNa_2\{Pr(H_2O)_7[Fe_4(H_2O)_{10}(B\text{-}\beta\text{-}AsW_9O_{33})_2]\}\cdot 21H_2O$ (2). $K_{14}[As_2W_{19}O_{67}(H_2O)]$ (0.264 g, 0.050 mmol), $FeCl_3\cdot 6H_2O$ (0.108 g, 0.399 mmol), $Pr(NO_3)_3\cdot 6H_2O$ (0.075 g, 0.172 mmol), L-leucine (0.058 g, 0.443 mmol), L-alanine (0.046 g, 0.517 mmol) and NaCl (0.105 g, 179.7 mmol) were successively added to 7 mL of water under stirring (pH = 2.17). The resulting suspension mixture was continuously stirred for 3 h, transferred to a 25 mL Teflon-lined steel autoclave, heated at 100 °C for 5 days and then cooled to room temperature. Eventually, light yellow virgate crystals of **2** were obtained by filtering, washed with distilled water and then dried at room temperature. Yield: *ca.* 25% (based on $K_{14}[As_2W_{19}O_{67}(H_2O)]$). Anal. calcd (found %) for $H_{76}As_2Fe_4KNa_2PrO_{104}W_{18}$ (**2**): H 1.36 (1.52), Na 0.81 (0.66), K 0.69 (0.88), Fe 3.95 (4.19), Pr 2.49 (2.65), W 58.58 (59.47). IR (KBr, cm^{-1}): 3422 (s), 1633 (s), 1466 (m), 1388 (m), 1354 (m), 963 (s), 885 (s), 815 (vs), 659 (s), 521 (m), 476 (w), 420 (w) (Fig. S1†).

$KNa_2\{Nd(H_2O)_7[Fe_4(H_2O)_{10}(B\text{-}\beta\text{-}AsW_9O_{33})_2]\}\cdot 21H_2O$ (3). $K_{14}[As_2W_{19}O_{67}(H_2O)]$ (0.264 g, 0.050 mmol), $FeCl_3\cdot 6H_2O$ (0.108 g, 0.399 mmol), $NdCl_3\cdot 6H_2O$ (0.073 g, 0.204 mmol), L-leucine (0.058 g, 0.443 mmol), L-alanine (0.046 g, 0.517 mmol) and NaCl (0.105 g, 179.7 mmol) were successively added to 7 mL of water under stirring (pH = 2.21). The resulting suspension mixture was continuously stirred for 3 h, transferred to a 25 mL Teflon-lined steel autoclave, heated at 100 °C for 5 days and then cooled to room temperature. Eventually, light yellow virgate crystals of **3** were obtained by filtering, washed with distilled water and then dried at room temperature. Yield: *ca.* 20% (based on $K_{14}[As_2W_{19}O_{67}(H_2O)]$). Anal. calcd (found %) for $H_{76}As_2Fe_4KNa_2NdO_{104}W_{18}$ (**3**): H 1.36 (1.51), Na 0.81 (0.62), K 0.69 (0.91), Fe 3.95 (4.16), Nd 2.55 (2.68), W 58.56 (59.57). IR (KBr, cm^{-1}): 3411 (s), 1627 (s), 1467 (m), 1398 (m), 1352 (m), 968 (s), 883 (s), 805 (vs), 672 (s), 512 (m), 485 (w), 430 (w) (Fig. S1†).

$KNa_2\{Sm(H_2O)_7[Fe_4(H_2O)_{10}(B\text{-}\beta\text{-}AsW_9O_{33})_2]\}\cdot 21H_2O$ (4). $K_{14}[As_2W_{19}O_{67}(H_2O)]$ (0.264 g, 0.050 mmol), $FeCl_3\cdot 6H_2O$ (0.106 g, 0.392 mmol), $SmCl_3\cdot 6H_2O$ (0.077 g, 0.211 mmol), L-leucine (0.058 g, 0.443 mmol), L-alanine (0.046 g, 0.517 mmol) and NaCl (0.105 g, 179.7 mmol) were successively added to 7 mL of water under stirring (pH = 2.21). The resulting suspension mixture was continuously stirred for 3 h, transferred to a 25 mL Teflon-lined steel autoclave, heated at 100 °C for 5 days and then cooled to room temperature. Eventually, light yellow virgate crystals of **4** were obtained by filtering, washed with

distilled water and then dried at room temperature. Yield: *ca.* 23% (based on $K_{14}[As_2W_{19}O_{67}(H_2O)]$). Anal. calcd (found %) for $H_{76}As_2Fe_4KNa_2SmO_{104}W_{18}$ (**4**): H 1.35 (1.57), Na 0.81 (0.68), K 0.69 (0.88), Fe 3.95 (4.10), Sm 2.66 (2.78), W 58.48 (59.47). IR (KBr, cm^{-1}): 3433 (s), 1636 (s), 1460 (m), 1391 (m), 1353 (m), 960 (s), 872 (s), 812 (vs), 658 (s), 518 (m), 479 (w), 429 (w) (Fig. S1†).

$[La(H_2O)_8]_2[Fe_4(H_2O)_8(L\text{-thr})_2][B\text{-}\beta\text{-}AsW_9O_{33}]_2\cdot 20H_2O$ (5). $K_{14}[As_2W_{19}O_{67}(H_2O)]$ (0.263 g, 0.049 mmol), $FeCl_3\cdot 6H_2O$ (0.103 g, 0.381 mmol), $LaCl_3\cdot 6H_2O$ (0.072 g, 0.204 mmol) and L-thr (0.053 g, 0.445 mmol) were successively added to 7 mL of water under stirring and the pH value of the mixture was carefully adjusted with a dilute NaOH solution (2 mol L^{-1}) to 2.24. The resulting suspension mixture was continuously stirred for 3 h, sealed in a 25 mL Teflon-lined steel autoclave, kept at 100 °C for 5 days and then cooled to room temperature. Light yellow flaky crystals of **5** were obtained by filtering, washed with distilled water and then dried at room temperature. Yield: *ca.* 22% $K_{14}[As_2W_{19}O_{67}(H_2O)]$. Anal. calcd (found %) for $C_8H_{106}As_2La_2Fe_4N_2O_{116}W_{18}$ (**5**): C 1.59 (1.81), H 1.77 (2.05), N 0.46 (0.68), Fe 3.69 (3.81), La 4.59 (4.83), W 54.72 (54.94). IR (KBr, cm^{-1}): 3425 (s), 1627 (s), 1502 (m), 1400 (m), 1352 (m), 961 (s), 897 (s), 811 (vs), 676 (s), 514 (m), 484 (w), 433 (w) (Fig. S1†).

$[Pr(H_2O)_8]_2[Fe_4(H_2O)_8(L\text{-thr})_2][B\text{-}\beta\text{-}AsW_9O_{33}]_2\cdot 20H_2O$ (6). The synthetic procedure was identical to **5**, but we used $PrCl_3\cdot 6H_2O$ (0.070 g, 0.197 mmol) instead of $LaCl_3\cdot 6H_2O$. Light yellow flaky crystals were collected. Yield: *ca.* 21% (based on $K_{14}[As_2W_{19}O_{67}(H_2O)]$). Anal. calcd (found %) for $C_8H_{106}As_2Pr_2Fe_4N_2O_{116}W_{18}$ (**6**): C 1.59 (1.83), H 1.77 (2.05), N 0.46 (0.69), Fe 3.69 (3.92), Pr 4.66 (4.87), W 59.69 (59.91). IR (KBr, cm^{-1}): 3417 (s), 1623 (s), 1494 (m), 1388 (m), 1352 (m), 957 (s), 893 (s), 807 (vs), 672 (s), 518 (m), 480 (w), 433 (w) (Fig. S1†).

$[Nd(H_2O)_8]_2[Fe_4(H_2O)_8(L\text{-thr})_2][B\text{-}\beta\text{-}AsW_9O_{33}]_2\cdot 20H_2O$ (7). The synthetic procedure was identical to **5**, but we used $NdCl_3\cdot 6H_2O$ (0.075 g, 0.209 mmol) instead of $LaCl_3\cdot 6H_2O$. Light yellow flaky crystals were collected. Yield: *ca.* 23% (based on $K_{14}[As_2W_{19}O_{67}(H_2O)]$). Anal. calcd (found %) for $C_8H_{106}As_2Nd_2Fe_4N_2O_{116}W_{18}$ (**7**): C 1.59 (1.88), H 1.76 (2.02), N 0.46 (0.67), Fe 3.69 (3.91), Nd 4.76 (4.88), W 54.62 (54.84). IR (KBr, cm^{-1}): 3405 (s), 1633 (s), 1499 (m), 1398 (m), 1352 (m), 960 (s), 897 (s), 810 (vs), 685 (s), 524 (m), 485 (w), 426 (w) (Fig. S1†).

$[Sm(H_2O)_8]_2[Fe_4(H_2O)_8(L\text{-thr})_2][B\text{-}\beta\text{-}AsW_9O_{33}]_2\cdot 20H_2O$ (8). The synthetic procedure was identical to **5**, but we used $SmCl_3\cdot 6H_2O$ (0.074 g, 0.203 mmol) instead of $LaCl_3\cdot 6H_2O$. Light yellow flaky crystals were collected. Yield: *ca.* 21% (based on $K_{14}[As_2W_{19}O_{67}(H_2O)]$). Anal. calcd (found %) for $C_8H_{106}As_2Sm_2Fe_4N_2O_{116}W_{18}$ (**8**): C 1.58 (1.79), H 1.76 (2.03), N 0.46 (0.68), Fe 3.68 (3.89), Sm 4.95 (5.12), W 54.51 (54.72). IR (KBr, cm^{-1}): 3417 (s), 1625 (s), 1502 (m), 1386 (m), 1350 (m), 961 (s), 895 (s), 810 (vs), 677 (s), 514 (m), 480 (w), 432 (w) (Fig. S1†).

$[Eu(H_2O)_8]_2[Fe_4(H_2O)_8(L\text{-thr})_2][B\text{-}\beta\text{-}AsW_9O_{33}]_2\cdot 20H_2O$ (9). The synthetic procedure was identical to **5**, but we used $Eu(NO_3)_3\cdot 6H_2O$ (0.096 g, 0.215 mmol) instead of $LaCl_3\cdot 6H_2O$. Light yellow flaky crystals were separated. Yield: *ca.* 30% (based on $K_{14}[As_2W_{19}O_{67}(H_2O)]$). Anal. calcd (found %) for $C_8H_{106}As_2Eu_2Fe_4\ N_2O_{116}W_{18}$ (**9**): C 1.58 (1.84), H 1.76 (2.01), N 0.46 (0.69), Fe 3.68 (3.87), Eu 5.00 (5.19), W 54.48 (54.71). IR (KBr, cm^{-1}): 3409 (s), 1629 (s), 1502 (m), 1386 (m), 1359 (m), 961 (s), 897 (s), 802 (vs), 685 (s), 522 (m), 478 (w), 433 (w) (Fig. S1†).

$[Gd(H_2O)_8]_2[Fe_4(H_2O)_8(L\text{-thr})_2][B\text{-}\beta\text{-}AsW_9O_{33}]_2\cdot 20H_2O$ (10). 10 was prepared according to the method of **5**, but $GdCl_3\cdot 6H_2O$ (0.076 g, 0.204 mmol) was used instead of $LaCl_3\cdot 6H_2O$. Light yellow flaky crystals were afforded. Yield: *ca.* 25% (based on $K_{14}[As_2W_{19}O_{67}\ (H_2O)]$). Anal. calcd (found %) for $C_8H_{106}As_2Gd_2Fe_4N_2O_{116}W_{18}$ (**10**): C 1.56 (1.83), H 1.76 (2.02), N 0.46 (0.68), Fe 3.67 (3.88), Gd 5.17 (5.39), W 54.39 (54.61). IR (KBr, cm^{-1}): 3419 (s), 1631 (s), 1500 (m), 1384 (m), 1353 (m), 962 (s), 891 (s), 804 (vs), 677 (s), 522 (m), 478 (w), 433 (w) (Fig. S1†).

$[Tb(H_2O)_9]_2[Fe_4(H_2O)_8(L\text{-thr})_2][B\text{-}\beta\text{-}AsW_9O_{33}]_2\cdot 20H_2O$ (11). The synthetic procedure was identical to **5**, but we used $TbCl_3\cdot 6H_2O$ (0.071 g, 0.190 mmol) instead of $LaCl_3\cdot 6H_2O$. Light yellow flaky crystals were collected. Yield: *ca.* 22% (based on $K_{14}[As_2W_{19}O_{67}\ (H_2O)]$). Anal. calcd (found %) for $C_8H_{106}As_2Tb_2Fe_4N_2O_{116}W_{18}$ (**11**): C 1.58 (1.81), H 1.76 (2.04), N 0.46 (0.66), Fe 3.67 (3.89), Tb 5.22 (5.42), W 54.36 (54.57). IR (KBr, cm^{-1}): 3402 (s), 1623 (s), 1498 (m), 1396 (m), 1352 (m), 969 (s), 898 (s), 815 (vs), 676 (s), 518 (m), 478 (w), 420 (w) (Fig. S1†).

$[Dy(H_2O)_8]_2[Fe_4(H_2O)_8(L\text{-thr})_2][B\text{-}\beta\text{-}AsW_9O_{33}]_2\cdot 20H_2O$ (12). The synthetic procedure was identical to **5**, but we used $Dy(NO_3)_3\cdot 6H_2O$ (0.098 g, 0.215 mmol) instead of $LaCl_3\cdot 6H_2O$. Light yellow flaky crystals were collected. Yield: *ca.* 22% (based on $K_{14}[As_2W_{19}O_{67}(H_2O)]$). Anal. calcd (found %) for $C_8H_{106}As_2Dy_2Fe_4\ N_2O_{116}W_{18}$ (**12**): C 1.58 (1.82), H 1.75 (1.96), N 0.46 (0.68), Fe 3.67 (3.88), Dy 5.33 (5.54), W 54.30 (54.52). IR (KBr, cm^{-1}): 3421 (s), 1621 (s), 1499 (w), 1399 (w), 1341 (w), 951 (s), 802 (s), 678 (w), 647 (m), 513 (w), 477 (w), 433 (w) (Fig. S1†).

$[Er(H_2O)_8]_2[Fe_4(H_2O)_8(L\text{-thr})_2][B\text{-}\beta\text{-}AsW_9O_{33}]_2\cdot 20H_2O$ (13). The synthetic procedure was identical to **5**, but we used $Er(NO_3)_3\cdot 6H_2O$ (0.098 g, 0.213 mmol) instead of $LaCl_3\cdot 6H_2O$. Light yellow flaky crystals were collected. Yield: *ca.* 22% (based on $K_{14}[As_2W_{19}O_{67}(H_2O)]$). Anal. calcd (found %) for $C_8H_{106}As_2Er_2Fe_4\ N_2O_{116}W_{18}$ (**13**): C 1.57 (1.83), H 1.75 (1.97), N 0.46 (0.67), Fe 3.66 (3.87), Er 5.48 (5.69), W 54.21 (54.43). IR (KBr, cm^{-1}): 3421 (s), 1621 (s), 1499 (w), 1399 (w), 1341 (w), 951 (s), 802 (s), 678 (w), 647 (m), 513 (w), 477 (w), 433 (w) (Fig. S1†).

X-ray crystallography

Single-crystal X-ray crystallographic analyses of **1–13** were performed using a Bruker APEX-II CCD sealed tube diffractometer at 296(2) K with graphite monochromated Mo Kα radiation (λ = 0.71073 Å). Their structures were determined using direct methods and difference Fourier techniques by the SHELXTL-97 program package.[11] Lorentz polarization and empirical absorption corrections were applied. All the non-H

atoms were anisotropically refined except for some O, C and N atoms and some water molecules, (details are seen in ESI†). In **1–4**, the K^+ and Ln^{3+} cations are disordered with a site occupancy of 0.5, which is determined according to the mass percentages of K^+ and Ln^{3+} cations from inductively coupled plasma atomic emission spectrometry and the magnitude of their anisotropic displacement parameters. Similar phenomena can be observed in some references.[12a,b] Notably, the structures of **5–13** contain chiral L-thr ligands, so theoretically their structures should be chiral. However, their structures are pseudo-centrosymmetric, *i.e.* most of the structure fits space group $P\bar{1}$, therefore, their structures were solved and refined in the centrosymmetric space group $P\bar{1}$. Such phenomena are rather common.[12c] Attempts to refine the structures of **5–13** in $P\bar{1}$ show the disorder around the chiral centre of L-thr (because we impose inversion on a chiral entity), as a result, the C1, C2, N1, O35 and O36 atoms on L-thr are disordered over two positions. In addition, some coordination water molecules on the Ln^{3+} cations in **5–13** are disordered over two positions. The C1, C2, N1, O35 and O36 atoms are refined isotropically. H atoms associated with C and N atoms were placed in calculated positions using a riding model and were refined isotropically using the default SHELXTL parameters. No H atoms associated with water molecules were located in the difference Fourier maps. The crystallographic data and structural refinement parameters for **1–13** are summarized in Table 1. The crystal structure details for **1–4** can be obtained from the Fachinformationszentrum Karlsruhe, 76344 Eggenstein-Leopoldshafen, Germany (fax: (+49)7247-808-666; e-mail: crystdata@fiz-karlsruhe.de) on quoting the depository numbers ICSD 429481, 429193, 429194 and 429482 for **1**, **2**, **3** and **4**. Crystallographic data for **5–13** reported in this paper have been deposited in the Cambridge Crystallographic Data Centre with CCDC 1048556–1048564 for **5–13**.

Results and discussion

Syntheses

In the past several years, some novel POM-based TLHDs with interesting structures and various properties have been reported,[8] however, reports on POM-based PTLHDs with amino acid ligands are still less developed.[12d,e] To the best of our knowledge, no AT-based PTLHD with amino acid ligands is reported to date although a family of organic–inorganic hybrid As^V-containing AT-based PTLHDs have been prepared by us in 2012,[9d] which offers us a good chance to explore the AT–TM–Ln–amino acid system. On the basis of our survey on the reported literatures, it can be found that the As^{III} atoms on the POM units possess a stereoactive lone pair of electrons, which can prevent the formation of the closed Keggin POM fragments, which helps to direct the aggregation of TM or Ln ions on the periphery of the lacunary AT building units and produce novel and complicated structures.[3b,f,h,6h–k] As a result, the As^{III}-containing dilacunary $K_{14}[As_2W_{19}O_{67}(H_2O)]$ AT was selected as the precursor. As we know, the dilacunary $[As_2W_{19}O_{67}(H_2O)]^{14-}$ polyoxoanion consists of two trilacunary $[B\text{-}\alpha\text{-}AsW_9O_{33}]^{9-}$ fragments linked by an octahedral $\{WO(H_2O)\}$ group. Previous experimental results have proved that the bridging $\{WO(H_2O)\}$ group is active and can be easily removed from the precursor leading to the isolation of trilacunary Keggin $[B\text{-}\alpha\text{-}AsW_9O_{33}]^{9-}$ fragments (Fig. 3a→c).[6b–d] Moreover, the trilacunary $[B\text{-}\alpha\text{-}AsW_9O_{33}]^{9-}$ fragment can be isomerized to the trilacunary $[B\text{-}\beta\text{-}AsW_9O_{33}]^{9-}$ fragment in the reaction processes (Fig. 3c→d).[6b,13] The formation of these trilacunary fragments tends to result in combination with TM or Ln ions. In addition, amino acid ligands have flexible N and O coordination sites, which favors coordination to TM or Ln ions by various coordination modes. It is well known that hydrothermal synthesis is an effective method for growing crystals of numerous inorganic or organic–inorganic hybrid materials,[14] therefore, we chose the hydrothermal technique to exploit this system. Based on these ideas, with the aim of discovering AT-based PTLHDs with amino acid ligands, we investigated the system containing $[As_2W_{19}O_{67}(H_2O)]^{14-}$, Fe^{3+}, and Ln^{3+} ions and amino acids. At the beginning, under 100 °C hydrothermal conditions in the presence of L-leucine and L-alanine, $K_{14}[As_2W_{19}O_{67}(H_2O)]$ was used to react with $FeCl_3{\cdot}6H_2O$ and $Pr(NO_3)_3{\cdot}6H_2O$ resulting in a 2-D pure inorganic AT-based PTLHD $KNa_2\{Pr(H_2O)_7[Fe_4(H_2O)_{10}(B\text{-}\beta\text{-}AsW_9O_{33})_2]\}{\cdot}21H_2O$ (**2**), and then $KNa_2\{Ln(H_2O)_7[Fe_4(H_2O)_{10}(B\text{-}\beta\text{-}AsW_9O_{33})_2]\}{\cdot}21H_2O$ [Ln = La^{III} (**1**), Nd^{III} (**3**), Sm^{III} (**4**)] were isolated (Fig. 3d→e), in which the Krebs' sandwich-type $[Fe_4(H_2O)_{10}(B\text{-}\beta\text{-}AsW_9O_{33})_2]^{6-}$ segment was seen. More interestingly, a $[Ln(H_2O)_7]^{3+}$ ion is disordered over both the upper and lower sides of a $[Fe_4(H_2O)_{10}(B\text{-}\beta\text{-}AsW_9O_{33})_2]^{6-}$ segment and has a site occupancy of 50% for each position. Unexpectedly, no L-leucine or L-alanine ligands were observed in **1–4**. During the course of preparing **1–4**, two aspects are worthy of mentioning here: (1) the pH of reaction system has an important effect on the formation of **1–4**. When the pH was lower than 1.5, the reported tetra-Fe^{III} encapsulated Krebs' sandwich-type AT $[Fe_4(H_2O)_{10}(B\text{-}\beta\text{-}AsW_9O_{33})_2]^{6-}$ was obtained.[15b] On the contrary, When the pH was higher than 2.5, the amorphous powders were formed. (2) The nature of the Ln ions also has a crucial influence on the formation of this series. When La^{3+} → Sm^{3+} ions were used in these conditions, the 2-D pure inorganic AT-based PTLHD $KNa_2\{Ln(H_2O)_7[Fe_4(H_2O)_{10}(B\text{-}\beta\text{-}AsW_9O_{33})_2]\}{\cdot}21H_2O$ [Ln = La^{III} (**1**), Pr^{III} (**2**), Nd^{III} (**3**), Sm^{III} (**4**)] can be obtained. Notably, the Ce^{III}-containing analogue of this series can be formed (it can be confirmed by the IR spectrum), but the quality of its crystal is not very good, hitherto, its crystal structure can't be resolved. When Eu^{3+} → Lu^{3+} ions were used in these conditions, the unknown powders were afforded. However, when we utilized L-thr to replace L-leucine and L-alanine, a family of organic–inorganic hybrid AT-based PTLHDs with L-thr ligands $[Ln(H_2O)_8]_2[Fe_4(H_2O)_8(L\text{-}thr)_2(B\text{-}\beta\text{-}AsW_9O_{33})_2]{\cdot}20H_2O$ [Ln = La^{III} (**5**), Pr^{III} (**6**), Nd^{III} (**7**), Sm^{III} (**8**), Eu^{III} (**9**), Gd^{III} (**10**), Tb^{III} (**11**), Dy^{III} (**12**), Er^{III} (**13**)] were successively obtained under similar conditions (Fig. 3d→f), in which two L-thr ligands in the $[Fe_4(H_2O)_8(L\text{-}thr)_2(B\text{-}\beta\text{-}AsW_9O_{33})_2]^{6-}$ subunit are substituted for

Table 1 X-ray diffraction crystallographic data and structure refinements for **1–13**

	1	**2**	**3**	**4**	**5**	**6**
Empirical formula	$H_{76}As_2Fe_4KNa_2LaO_{104}W_{18}$	$H_{76}As_2Fe_4KNa_2PrO_{104}W_{18}$	$H_{76}As_2Fe_4KNa_2NdO_{104}W_{18}$	$H_{76}As_2Fe_4KNa_2SmO_{104}W_{18}$	$C_8H_{106}As_2La_2Fe_4N_2O_{116}W_{18}$	$C_8H_{106}As_2Pr_2Fe_4N_2O_{116}W_{18}$
Formula weight	5647.14	5649.14	5652.29	5658.58	6047.31	6051.31
Crystal system	Triclinic	Triclinic	Triclinic	Triclinic	Triclinic	Triclinic
Space group	$P\bar{1}$	$P\bar{1}$	$P\bar{1}$	$P\bar{1}$	$P\bar{1}$	$P\bar{1}$
a, Å	12.650(10)	12.7027(13)	12.7021(14)	12.671(5)	12.6669(13)	12.6523(18)
b, Å	13.180(10)	13.2756(14)	13.2675(14)	13.247(5)	13.5788(13)	13.5456(19)
c, Å	15.709(12)	15.6850(17)	15.6418(17)	15.610(6)	16.3488(17)	16.272(2)
α, °	79.285(14)	78.960(2)	78.908(2)	78.699(6)	107.303(2)	107.169(2)
β, °	89.130(15)	89.022(2)	88.859(2)	88.927(6)	99.720(2)	99.786(2)
γ, °	65.290(12)	65.272(2)	65.171(2)	65.208(6)	96.736(2)	96.861(2)
V, Å^{-3}	2332(3)	2352.2(4)	2342.2(4)	2326.6(16)	2604.0(5)	2582.7(6)
Z	1	1	1	1	1	1
μ, mm^{-1}	24.026	23.885	24.021	24.255	21.889	22.185
F(000)	2508	2510	2510	2513	2712	2716
T, K	296(2)	296(2)	296(2)	296(2)	296(2)	296(2)
Limiting indices	$-14 \le h \le 15$ $-15 \le k \le 15$ $-18 \le l \le 16$	$-15 \le h \le 15$ $-15 \le k \le 15$ $-18 \le l \le 18$	$-15 \le h \le 15$ $-15 \le k \le 15$ $-18 \le l \le 13$	$-15 \le h \le 15$ $-15 \le k \le 15$ $-14 \le l \le 18$	$-15 \le h \le 15$ $-16 \le k \le 8$ $-18 \le l \le 19$	$-15 \le h \le 15$ $-9 \le k \le 16$ $-19 \le l \le 19$
No. of reflections collected	11 198	11 716	11 222	11 716	13 131	12 556
No. of independent reflections	7882	8104	7942	8031	8975	8830
R_{int}	0.0506	0.0359	0.0349	0.0403	0.0413	0.0416
Data/restrains/parameters	7882/133/582	8104/31 /582	7942/79/577	8031/7/582	8975/24/656	8830/79/656
GOFon F^2	1.039	1.025	1.067	1.020	1.005	1.023
Final R indices	R_1 = 0.0738	R_1 = 0.0443	R_1 = 0.0599	R_1 = 0.0458	R_1 = 0.0483	R_1 = 0.0586
[$I > 2\sigma(I)$]	wR_2 = 0.2009	wR_2 = 0.1228	wR_2 = 0.1658	wR_2 = 0.1196	wR_2 = 0.1196	wR_2 = 0.1604
R Indices (all data)	R_1 = 0.1072 wR_2 = 0.2301	R_1 = 0.0524 wR_2 = 0.1281	R_1 = 0.0737 wR_2 = 0.1738	R_1 = 0.0530 wR_2 = 0.1242	R_1 = 0.0563 wR_2 = 0.1238	R_1 = 0.0699 wR_2 = 0.1682
Largest diff. peak and hole, e Å^{-3}	3.940, −5.195	3.972, −2.459	3.960, −3.374	3.005, −2.694	2.138, −3.669	4.557, −4.440

Table 1 *(Contd.)*

7	8	9	10	11	12	13
$C_8H_{106}As_2Nd_2Fe_4N_2O_{116}W_{18}$	$C_8H_{106}As_2Sm_2Fe_4N_2O_{116}W_{18}$	$C_8H_{106}As_2Eu_2Fe_4N_2O_{116}W_{18}$	$C_8H_{106}As_2Gd_2Fe_4N_2O_{116}W_{18}$	$C_8H_{106}As_2Tb_2Fe_4N_2O_{116}W_{18}$	$C_8H_{106}As_2Dy_2Fe_4N_2O_{116}W_{18}$	$C_8H_{106}As_2Er_2Fe_4N_2O_{116}W_{18}$
6057.79	6070.19	6073.41	6083.99	6087.33	6094.49	6104.01
Triclinic	Triclinic	Triclinic	Triclinic	Triclinic	Triclinic	Triclinic
$P\bar{1}$	$P\bar{1}$	$P\bar{1}$	$P\bar{1}$	$P\bar{1}$	$P\bar{1}$	$P\bar{1}$
12.6668(10)	12.6577(16)	12.6292(14)	12.6230(7)	12.6063(13)	12.6307(11)	12.5799(9)
13.5691(11)	13.5693(17)	13.5134(15)	13.5118(8)	13.4464(14)	13.5293(11)	13.4462(10)
16.3027(13)	16.278(2)	16.1999(18)	16.1922(9)	16.0241(17)	16.1950(14)	16.0508(12)
107.1270(10)	107.165(2)	106.993(2)	106.7890(10)	106.473(2)	106.8530(10)	106.5070(10)
99.7630(10)	99.801(2)	99.753(2)	99.7550(10)	99.828(2)	99.7760(10)	99.7760(10)
96.8760(10)	96.896(2)	97.011(2)	97.1520(10)	97.290(2)	97.1530(10)	97.3250(10)
2595.8(4)	2588.9(6)	2562.3(5)	2561.4(3)	2522.0(5)	2565.5(4)	2520.2(3)
1	1	1	1	1	1	1
22.134	22.325	22.635	22.713	23.155	22.840	23.434
2717	2722	2724	2726	2728	2730	2734
296(2)	296(2)	296(2)	296(2)	296(2)	296(2)	296(2)
$-15 \leq h \leq 15$	$-15 \leq h \leq 14$	$-14 \leq h \leq 15$	$-14 \leq h \leq 15$	$-14 \leq h \leq 14$	$-14 \leq h \leq 15$	$-13 \leq h \leq 14$
$-16 \leq k \leq 12$	$-16 \leq k \leq 8$	$-16 \leq k \leq 15$	$-16 \leq k \leq 15$	$-11 \leq k \leq 15$	$-16 \leq k \leq 15$	$-15 \leq k \leq 15$
$-17 \leq l \leq 19$	$-17 \leq l \leq 19$	$-19 \leq l \leq 15$	$-19 \leq l \leq 10$	$-19 \leq l \leq 18$	$-19 \leq l \leq 14$	$-18 \leq l \leq 19$
13 219	12 546	12 504	12 855	12 412	12 802	12 430
8997	8797	8691	8773	8575	8740	8566
0.0379	0.0453	0.0372	0.0379	0.0358	0.0328	0.0478
8997/73/655	8797/120/656	8691/186/651	8773/37/655	8575/96/654	8740/37/654	8566/192/654
1.027	1.023	1.048	1.024	1.039	1.039	1.038
$R_1 = 0.0502$	$R_1 = 0.0602$	$R_1 = 0.0681$	$R_1 = 0.0507$	$R_1 = 0.0569$	$R_1 = 0.0489$	$R_1 = 0.0709$
$wR_2 = 0.1235$	$wR_2 = 0.1578$	$wR_2 = 0.1836$	$wR_2 = 0.1292$	$wR_2 = 0.1459$	$wR_2 = 0.1233$	$wR_2 = 0.1867$
$R_1 = 0.0572$	$R_1 = 0.0718$	$R_1 = 0.0739$	$R_1 = 0.0589$	$R_1 = 0.0641$	$R_1 = 0.0543$	$R_1 = 0.0778$
$wR_2 = 0.1273$	$wR_2 = 0.1656$	$wR_2 = 0.1890$	$wR_2 = 0.1341$	$wR_2 = 0.1507$	$wR_2 = 0.1265$	$wR_2 = 0.1932$
2.884, −3.923	4.027, −4.951	4.385, −5.703	2.473, −4.361	3.563, −5.720	2.647, −4.784	4.397, −5.990

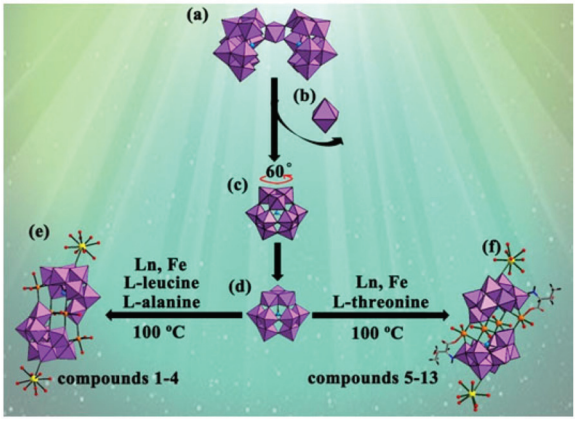

Fig. 3 The formation processes of **1–13**. (a) The precursor $[As_2W_{19}O_{67}(H_2O)]^{14-}$; (b) the removable $\{WO_6\}$ octahedron; (c) the $[B\text{-}\alpha\text{-}AsW_9O_{33}]^{9-}$ segment existing in the precursor; (d) the $[B\text{-}\beta\text{-}AsW_9O_{33}]^{9-}$ segment in **1–13**; (e) polyhedral and ball-and-stick view of **1–4**; (f) polyhedral and ball-and-stick view of **5–13**.

two aqueous ligands in the $[Fe_4(H_2O)_{10}(B\text{-}\beta\text{-}AsW_9O_{33})_2]^{6-}$ segment and two $[Ln(H_2O)_8]^{3+}$ cations are supported by both the upper and lower sides of the $[Fe_4(H_2O)_8(L\text{-thr})_2(B\text{-}\beta\text{-}AsW_9O_{33})_2]^{6-}$ subunit. Hitherto, we haven't found the reaction rule that determines what amino acid ligands can graft to TM or Ln cations in this reaction system. This work is being extensively performed in our lab.

Structural description

The analytical results of the single-crystal X-ray diffraction reveal that **1–4** are isostructural and both crystallize in the triclinic space group $P\bar{1}$. As a result, only the structure of **2** is described in detail. The molecular structural unit of **2** is composed of a Fe–Pr heterometallic $\{[Pr(H_2O)_7][Fe_4(H_2O)_{10}(B\text{-}\beta\text{-}AsW_9O_{33})_2]\}^{3-}$ subunit (**2a**), a K^+ cation, two Na^+ cations and twenty-one water molecules of crystallization (Fig. 4a). As far as we know, this tetra-Fe^{III} substituted sandwich-type AT $\{[Pr(H_2O)_7][Fe_4(H_2O)_{10}(B\text{-}\beta\text{-}AsW_9O_{33})_2]\}^{3-}$ fragment with a supporting $[Pr(H_2O)_7]^{3+}$ cation in **2** is unseen in the field of POM chemistry, although a classical tetra-Fe^{III} substituted sandwich-type $[Mn_4(H_2O)_2(B\text{-}\alpha\text{-}SiW_9O_{34})_2]^{12-}$ subunit with two supporting $[Ce(H_2O)_7]^{3+}$ cations was seen in an inorganic aggregate $K_4Na_2[\{Ce(H_2O)_7\}_2Mn_4Si_2W_{18}O_{68}(H_2O)_2]\cdot 21.5H_2O$ reported by Wang *et al.* in 2007.[8n] In **2a**, the $[Fe_4(H_2O)_{10}(B\text{-}\beta\text{-}AsW_9O_{33})_2]^{6-}$ segment retains a Krebs' sandwich-type structure with idealized C_{2h} symmetry, which consists of two identical $[B\text{-}\beta\text{-}AsW_9O_{33}]^{9-}$ moieties which are connected by two inner $[Fe(H_2O)_2]^{3+}$ and two outer $[Fe(H_2O)_3]^{3+}$ groups. In the $[B\text{-}\beta\text{-}AsW_9O_{33}]^{9-}$ fragment, the As^{III} atom possesses an unshared pair of electrons and exhibits a tri-coordinate environment defined by three μ_4-oxygen atoms from three $\{W_3O_{13}\}$ groups with As–O distances of 1.788(8)–1.837(10) Å. Moreover, all the W centers exhibit the octahedral coordination environment with W–O distances of 1.702(10)–2.409(9) Å. In **2a**, there are two crystallographically unique Fe^{3+} cations

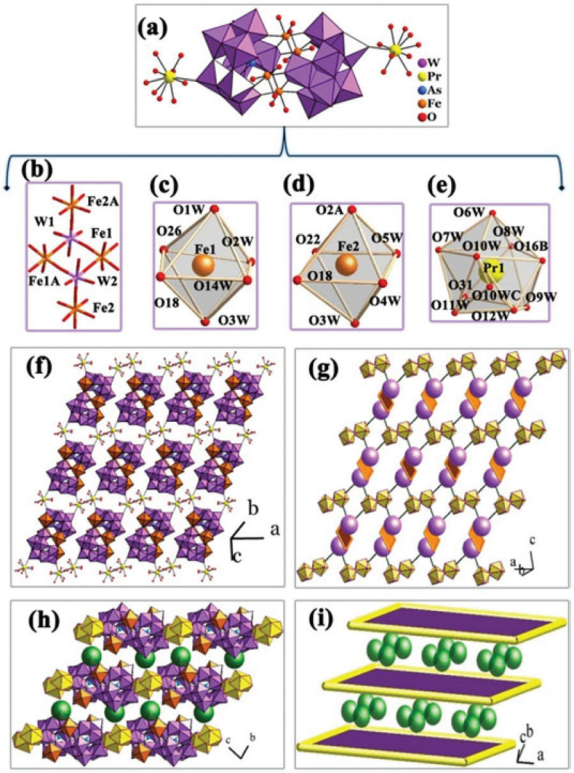

Fig. 4 (a) Combined polyhedral and ball-and-stick view of **2a**; (b) the connection between four Fe^{3+} ions by two W atoms in **2a**; (c) the octahedral environment of the $Fe1^{3+}$ ion in **2a**; (d) the octahedral geometry of the $Fe2^{3+}$ ion in **2a**; (e) the coordination environment of the $Pr1^{3+}$ ion in **2a**; (f) the 2-D network of **2**; (g) the simplified 2-D network; (h) the 3-D packing alignment of **2** with stuffing Na^+ ions; (i) the simplified 3-D packing structure. The atoms with the suffix A are generated by the symmetry operation where A: $2-x, 1-y, z$, B: $2-x, -y, 1-z$, C: $1-x, -y, 1-z$. Crystal water molecules are omitted for clarity.

($Fe1^{3+}$ and $Fe2^{3+}$) (Fig. 4b). The two inner Fe^{3+} ($Fe1^{3+}$ and $Fe1A^{3+}$) cations possess two terminal H_2O ligands while the two outer Fe^{3+} ($Fe2^{3+}$ and $Fe2A^{3+}$) cations have three terminal H_2O ligands. Although both the $Fe1^{3+}$ and $Fe2^{3+}$ cations adopt the octahedral geometry, their coordination environments are somewhat different: the octahedron of the $Fe1^{3+}$ cation is defined by four O atoms from two $[B\text{-}\beta\text{-}AsW_9O_{33}]^{9-}$ moieties [Fe–O: 1.918(9)–1.954(10) Å] and two water ligands [Fe–O: 2.134(10)–2.144(10) Å] (Fig. 4c), whereas the octahedron of the $Fe2^{3+}$ cation is constituted by three O atoms from two $[B\text{-}\beta\text{-}AsW_9O_{33}]^{9-}$ moieties [Fe–O: 1.933(9)–1.988(10) Å] and three water ligands [Fe–O: 2.064(10)–2.091(11) Å] (Fig. 4d). This Krebs' sandwich-type structure was first discovered in $[Sb_2W_{22}O_{74}(OH)_2]^{12-}$ comprising two trivacant Keggin-type $[B\text{-}\beta\text{-}SbW_9O_{33}]^{9-}$ segments connected by two internal $[WO_2]^{2+}$ and two external $[WO_2(OH)]^+$ groups by Krebs and co-workers in 1997.[15a] In 2002, Kortz *et al.* employed the $[\alpha\text{-}AsW_9O_{33}]^{9-}$ precursor to react with Fe^{3+} ions in a pH = 3.0 aqueous solution and synthesized the tetra-Fe^{III} encapsulated Krebs' sandwich-type AT $[Fe_4(H_2O)_{10}(B\text{-}\beta\text{-}AsW_9O_{33})_2]^{6-}$ with crystal structure determination.[15b] It's worth pointing out that the $Pr1^{3+}$ cation

splits to two positions with a 50% site occupancy of each position (Fig. S2†). Furthermore, the $Pr1^{3+}$ cation links to one terminal O atom from one trivacant Keggin $[B\text{-}\beta\text{-}AsW_9O_{33}]^{9-}$ fragment [Pr–O: 2.605(9) Å], one terminal O atom from the other trivacant Keggin $[B\text{-}\beta\text{-}AsW_9O_{33}]^{9-}$ fragment [Pr–O: 2.458(11) Å], two μ_2-O atoms from two H_2O ligands [Pr–O: 2.03(3)–2.45(3) Å] and six terminal O atoms from terminal H_2O ligands [Pr–O: 2.41(3)–2.61(2) Å] to complete its ten-coordinate geometry (Fig. 4e). Interestingly, adjacent $[Fe_4(H_2O)_{10}(B\text{-}\beta\text{-}AsW_9O_{33})_2]^{6-}$ subunits are connected with each other by the Pr^{3+} linkers to result in a beautiful two-dimensional (2-D) network (Fig. 4f). From the view of simplification, the $[B\text{-}\beta\text{-}AsW_9O_{33}]^{9-}$ moieties are treated as purple spheres and the tetra-Fe^{III} units are looked on as orange planes, as a result, an aesthetical representation of a 2-D layer is presented (Fig. 4g). The Krebs' sandwich-type AT subunits $[Fe_4(H_2O)_{10}(B\text{-}\beta\text{-}AsW_9O_{33})_2]^{6-}$ and the complicated connection mode between the Krebs' sandwich-type AT subunits and the splitting Pr^{3+} ions are clearly visualized in the simplified 2-D network. What's more, the interesting 3-D packing architecture is illustrated in Fig. 4h, it can be clearly seen that stuffing Na^+ ions are distributed on the interspace between adjacent 2-D layers and the 3-D packing architecture was further simplified by considering the 2-D layers as the planes (Fig. 4i).

5–13 are isomorphous and they all crystallize in the triclinic space group $P\bar{1}$. Hence, the structural description is exemplified by **5** at length. Although **2** and **5** belong to the same space group, their structures are distinct from each other and the differences will be discussed in the following description. Structurally, the basic molecular structural unit $[La(H_2O)_8]_2[Fe_4(H_2O)_8(\text{L-thr})_2(B\text{-}\beta\text{-}AsW_9O_{33})_2]\cdot 20H_2O$ of **5** is composed of an organic–inorganic Fe–La heterometallic $[La(H_2O)_8]_2[Fe_4(H_2O)_8(\text{L-thr})_2(B\text{-}\beta\text{-}AsW_9O_{33})_2]$ subset (**5a**) and twenty lattice water molecules. From Fig. 5a and b, it is clear to see that the tetra-Fe^{III} substituted Krebs' sandwich-type AT $[Fe_4(H_2O)_{10}(B\text{-}\beta\text{-}AsW_9O_{33})_2]^{6-}$ subunit associates with two "attached" nine-coordinate $[La(H_2O)_8]^{3+}$ ions through two terminal O atoms from the $[B\text{-}\beta\text{-}AsW_9O_{33}]^{9-}$ segments, giving rise to the interesting $[La(H_2O)_8]_2[Fe_4(H_2O)_8(\text{L-thr})_2(B\text{-}\beta\text{-}AsW_9O_{33})_2]$ hybrid, in which two L-thr ligands coordinate to two external Fe^{3+} ions situated on the sandwich belt of the Krebs-type subunit *via* two O atoms. To the best of our knowledge, such a Fe–Ln heterometallic AT with L-thr ligands was unseen although similar tungstoantimonate-based TM–Ln heterometallic hybrids have been discovered.[12a] In $[Fe_4(H_2O)_8(\text{L-thr})_2(B\text{-}\beta\text{-}AsW_9O_{33})_2]^{6-}$, two identical $[B\text{-}\beta\text{-}AsW_9O_{33}]^{9-}$ moieties (Fig. 5c) are bridged by the central symmetric organic–inorganic $[Fe^{III}_4(\text{L-thr})_2]^{12+}$ group (Fig. 5d). In each $[B\text{-}\beta\text{-}AsW_9O_{33}]^{9-}$ fragment, the As^{III} atom also exhibits a tri-coordinate trigonal pyramid defined by three μ_4-oxygen atoms from three W_3O_{13} triads with As–O distances of 1.804(10)–1.816(10) Å, and all W centers exhibit the $\{WO_6\}$ octahedra with W–O distances of 1.714(10)–2.391(11) Å. In $[Fe_4(H_2O)_8(\text{L-thr})_2(B\text{-}\beta\text{-}AsW_9O_{33})_2]^{6-}$, the coordination environments of the inner $Fe1^{3+}$ ($Fe1A^{3+}$) ions and the outer $Fe2^{3+}$ ($Fe2A^{3+}$) ions are also somewhat different. The coordination geometry of the inner $Fe1^{3+}$ ion is built by two O atoms from one $[B\text{-}\beta\text{-}AsW_9O_{33}]^{9-}$ fragment [Fe–O: 1.933(10)–1.950(10) Å], two O atoms from the other $[B\text{-}\beta\text{-}AsW_9O_{33}]^{9-}$ fragment [Fe–O: 1.956(10)–1.962(10) Å] and two O atoms from two terminal H_2O ligands [Fe–O: 2.121(12)–2.144(11) Å] (Fig. 5f). Whereas the coordination geometry of the $Fe2^{3+}$ ion is defined by one O atom from the L-thr ligand [Fe–O: 2.049(12) Å], one O atom from one $[B\text{-}\beta\text{-}AsW_9O_{33}]^{9-}$ fragment [Fe–O: 1.983(11) Å], two O atoms from the other $[B\text{-}\beta\text{-}AsW_9O_{33}]^{9-}$ fragment [Fe–O: 1.932(11)–1.952(11) Å] and two O atoms from two terminal H_2O molecules [Fe–O: 2.066(14)–2.083(14) Å] (Fig. 5g).

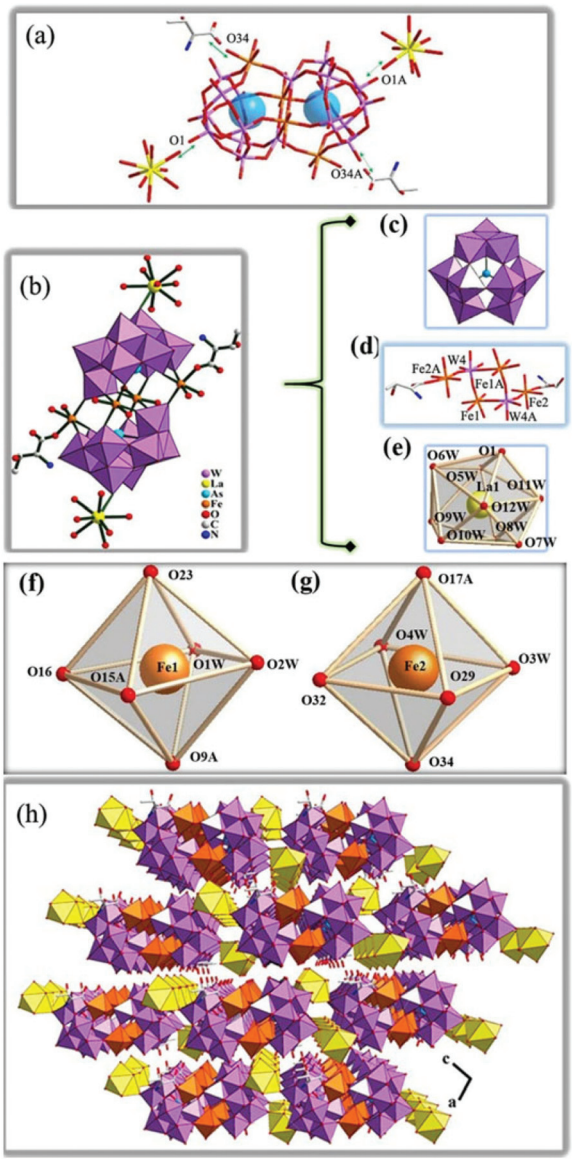

Fig. 5 (a) The wire view of **5a**; (b) combined polyhedral and ball-and-stick view of **5a**; (c) the view of the $[B\text{-}\beta\text{-}AsW_9O_{33}]^{9-}$ segment in **5a**; (d) the connection between four Fe^{3+} ions by two W atoms in **5a**; (e) the coordination environment of the $La1^{3+}$ ion in **5a**; (f) the octahedral environment of the $Fe1^{3+}$ ion in **5a**; (g) the octahedral environment of the $Fe2^{3+}$ ion in **5a**; (h) the 3-D packing architecture of **5**. The atoms with the suffix A are generated by the symmetry operation where A: $1-x, 1-y, 2-z$. Crystal water molecules are omitted for clarity.

In addition, the La1^{3+} cation (Fig. 5e) in **5** achieves the monocapped square antiprismatic 9-fold coordination by attachment to a terminal O atom from the trivacant Keggin [B-β-AsW$_9$O$_{33}$]$^{9-}$ fragment [La–O: 2.547(10) Å] and eight O atoms from eight aqua-oxygen ligands [La–O: 2.521(18)–2.62(3) Å], which is somewhat different from the tricapped square prism geometry of the Pr^{3+} ion in **2**. Comparing **5** and **2**, two obvious discrepancies are observed: (a) **2** is a purely inorganic 2-D structure while **5** is a discrete organic–inorganic hybrid containing a tetra-Fe^{III} [Fe$_4$(H$_2$O)$_8$(L-thr)$_2$]$^{12-}$ (Fig. 5d) sandwiched [La(H$_2$O)$_8$]$_2$-[Fe$_4$(H$_2$O)$_8$(L-thr)$_2$(B-β-AsW$_9$O$_{33}$)$_2$] moiety. (b) The Pr1^{3+} cation in **2** inhabits in a distorted nona-coordinate tricapped square prism, in contrast, the La1^{3+} cation in **5** adopts a nona-coordinate severely distorted monocapped square antiprism configuration. The 3-D packing structure of **5** is shown in Fig. 5h.

IR spectra

The IR spectra of **1–3** have been recorded between 4000 and 400 cm^{-1} with KBr pellets (Fig. S1†) and the low wave-number regions display four characteristic terminal ν_{as}(W–O$_t$), and ν_{as}(As–O$_a$), corner-sharing ν_{as}(W–O$_b$) and edge-sharing ν_{as}(W–O$_c$) asymmetric stretching vibration bands derived from the Keggin-type AT skeleton, which are observed at 960, 881, 802, and 662 cm^{-1} for **1**, 963, 885, 815, and 659 cm^{-1} for **2**, 968, 883, 805, and 672 cm^{-1} for **3**, 960, 872, 812, and 658 cm^{-1} for **4**, 961, 897, 811, and 676 cm^{-1} for **5**, 957, 893, 807, and 672 cm^{-1} for **6**, 960, 897, 810, and 683 cm^{-1} for **7**, 961, 895, 810, and 677cm^{-1} for **8**, 961, 897, 802, and 685 cm^{-1} for **9**, 962, 891, 804, and 677 cm^{-1} for **10**, 969, 898, 818, and 676 cm^{-1} for **11**, 960, 896, 817, and 682 cm^{-1} for **12**, and 967, 894, 816, and 680 cm^{-1} for **13**, respectively. It's easy to see that the IR spectra of **1–13** are very similar in the low wave-number regions, which may be due to the presence of the trivacant Keggin [B-β-AsW$_9$O$_{33}$]$^{9-}$ fragments in their skeletons. In the high wave-number region, all show a broad band at 3419–3448 cm^{-1} and a strong absorption band at 1626–1640 cm^{-1}, which are assigned to the stretching and bending vibration modes of water molecules, respectively. But for **5–13** with L-thr ligands, the ν(C–O) absorption bands of the L-thr ligands are overlapped by the intense bending vibration bands of the water molecules. The bands at 1336–1354 cm^{-1} are indicative of the ν(C–N) vibration. It should be noted that apparent shifts of the ν_{as}(W–O$_t$), ν_{as}(As–O$_a$), ν_{as}(W–O$_b$) and ν_{as}(W–O$_c$) vibration frequencies occur by comparing the IR data of **1–13** with those of the precursor K$_{14}$[As$_2$W$_{19}$O$_{67}$(H$_2$O)] [951, 891, 796 and 751 cm^{-1} for ν_{as}(W–O$_t$), ν_{as}(As–O$_a$), ν_{as}(W–O$_b$) and ν_{as}(W–O$_c$), respectively],[16] which may result from the transformation of [As$_2$W$_{19}$O$_{67}$(H$_2$O)]$^{14-}$ → [B-β-AsW$_9$O$_{33}$]$^{9-}$ as well as the embedding of the tetra-Fe^{III} [Fe$^{III}_4$(H$_2$O)$_8$(L-thr)$_2$]$^{12+}$ cluster into the defects of two [B-β-AsW$_9$O$_{33}$]$^{9-}$ fragments. In comparison with the IR spectra of **1–4**, the appearance of the weak vibration peaks of **5–13** suggests the implanting of L-thr ligands onto the two external Fe^{3+} ions of the [Ln(H$_2$O)$_8$]$_2$[Fe$_4$(H$_2$O)$_8$(L-thr)$_2$(B-β-AsW$_9$O$_{33}$)$_2$] subunits. But, the Ln–O stretching vibrations can't be observed, which may be relevant to the dominant ionic interactions between trivacant POM fragments and Ln^{III} ions.[17]

Photoluminescence (PL) properties

The highly emissive Y$_2$O$_3$:Eu^{III} material is a significant discovery in the Ln luminescence field.[18] Since Finnish researchers used Eu^{III} and Tb^{III} containing polyaminocarboxylates and β-diketonates as bioprobes in time-resolved luminescence (TRL) immunoassays, continuous investigations on luminescent coordination compounds sprang up.[19] Nowadays, Ln coordination compounds highlight the fascinating and outstanding luminescence properties in light conversion fields such as light-emitting diodes, sensory probes, plasma displays, medicinal analyses, cell imaging as well as monitoring drug delivery,[20] which benefit from the eminent electronic properties of Ln cations: the shielding of the 4f orbitals by the filled 5s^{2}5p^6 subshells.[21] It should be noted that the photoexcitation of the O → M (M = Mo or W) transitions of POM units are able to give rise to intramolecular energy transfer from the O → M excited states to the excited energy levels of Ln^{III} ions, which then sensitizes the emission of the Ln cations. Therefore, the intramolecular energy transfer from POMs to Ln cations can occur *via* a ligand-to-metal charge transfer (LMCT) route.[22] The luminescence properties and mechanism of energy transfer from the ligand to the metal of some POM-based Ln derivatives have been widely studied.[22] Hence, the PL behaviors of **9** and **11** in the solid state have been investigated at room temperature. The emission spectrum of **9** was conducted under a maximum excitation wavelength at 394 nm. The emission spectrum of **9** is composed of the first excited state, ^{5}D$_0$, and the ground septet, ^{7}F$_J$ (J = 0–4) of the Eu^{III} cation.[23a] Five characteristic transitions from the first excited ^{5}D$_0$ state of Eu^{III} to the ground-state ^{7}F$_J$ manifold are evident and the apparent peak maxima appear at approximately 558, 585, 617, 651 and 697 nm for J = 0, 1, 2, 3 and 4, respectively (Fig. 6a). These data are in accordance with the previous results.[9d,23c–f] Formally, the ^{5}D$_0$ → ^{7}F$_0$ transition reveals the symmetry-forbidden emission, which is severely forbidden in a field of symmetry. Interestingly, the presence of the ^{5}D$_0$ → ^{7}F$_0$ transition at 558 nm can still be observed in **9**, demonstrating that the Eu^{III} ions are located in the lower symmetric ligand field, which coincides with the monocapped square antiprismatic geometry of the Eu^{III} ions. It is concluded that the magnetic-dipolar ^{5}D$_0$ → ^{7}F$_{1,3}$ transitions are insensitive to the local microenvironments whereas the electric-dipolar ^{5}D$_0$ → ^{7}F$_{2,4}$ transitions are extraordinarily sensitive to the local microenvironments.[23e,24] In general, the emission intensity of the magnetic dipole ^{5}D$_0$ → ^{7}F$_1$ transition scarcely varies with the strength of the ligand field exerted on the Eu^{III} ion, whereas the intensity of the electric dipole ^{5}D$_0$ → ^{7}F$_2$ transition is highly sensitive to the chemical bonds in the neighborhood of the Eu^{III} ions.[12a] The emission intensity of the magnetic dipole ^{5}D$_0$ → ^{7}F$_1$ transitions dominates in a centrosymmetric environment, in contrast, the ^{5}D$_0$ → ^{7}F$_2$ transition is the strongest in a noncentrosymmetric situation.[9d,25] Thereby, the I(^{5}D$_0$ → ^{7}F$_2$)/I(^{5}D$_0$ → F$_1$) ratio is generally used as a criterion of

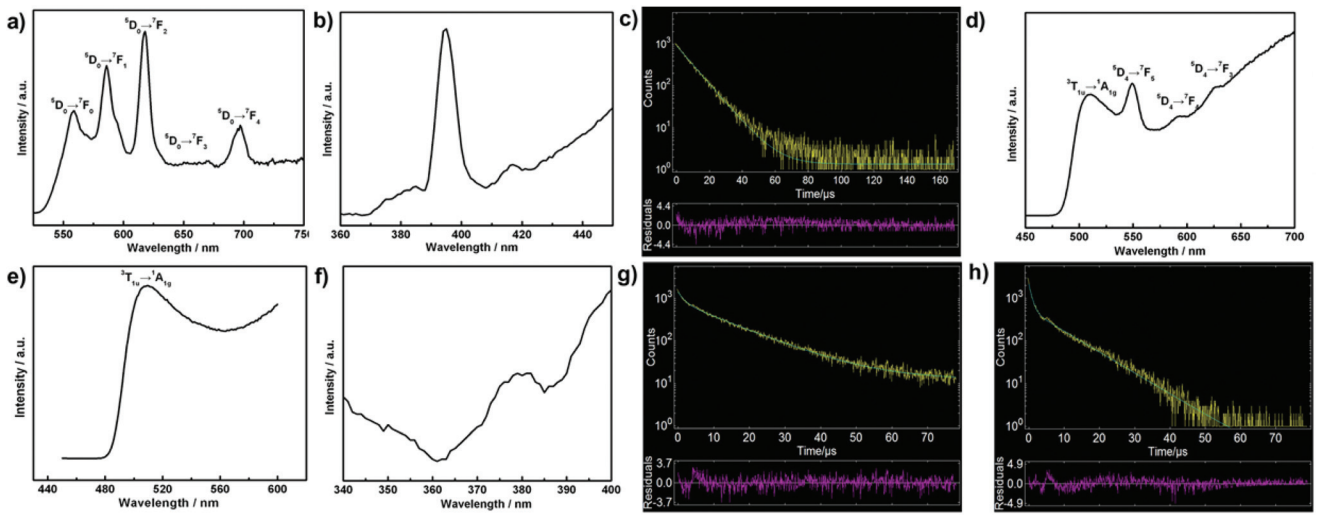

Fig. 6 (a) The emission spectrum of **9** under excitation at 394 nm at room temperature. (b) The excitation spectrum of **9** monitored at the Eu^{III} $^5D_0 \rightarrow {}^7F_2$ transition (617 nm) at room temperature. (c) The luminescence decay curve of **9**. (d) The emission spectrum of **11** under excitation at 379 nm at room temperature. (e) The emission spectrum of the precursor $K_{14}[As_2W_{19}O_{67}(H_2O)]$ under excitation at 379 nm at room temperature. (f) The excitation spectrum of **11** monitored at the intense $^5D_4 \rightarrow {}^7F_5$ transition (549 nm) of the Tb^{III} ion. (g) The luminescence decay curve of **11**. (h) The luminescence decay curve of the precursor $K_{14}[As_2W_{19}O_{67}(H_2O)]$.

the coordination environment and site symmetry of the Eu^{III} ions.[26] The value of this intensity ratio for **9** is *ca.* 1.3 reflecting the comparatively low site symmetry of the Eu^{III} ion, and it is also in good agreement with the distorted monocapped square antiprism geometry of the Eu^{III} cation. Moreover, the excitation spectrum of **9** monitored at the Eu^{III} $^5D_0 \rightarrow {}^7F_2$ transition (617 nm) contains a broad band and several weak bands (Fig. 6b). The broad band at 394 nm is assigned to the $^7F_0 \rightarrow {}^5L_6$ transition of the Eu^{III} intra-$4f^6$ ion, the weak bands between 375–384 nm correspond to the $^7F_0 \rightarrow {}^5G_{0-4}$ transitions, whereas the weak band at 416 nm is attributed to the $^7F_0 \rightarrow {}^5D_3$ transitions.[23a,b] The $^5D_0$ lifetime curve of the Eu^{III} ion was monitored under excitation at 394 nm and the more intense emission at 617 nm ($^5D_0 \rightarrow {}^7F_2$) (Fig. 6c), which can be well fitted to a single exponential function [$I = A\exp(-t/\tau)$], yielding a lifetime value (τ) of 9.51 μs, a pre-exponential factor (A) of 934.17 and an agreement factor (χ^2) of 1.087. In comparison with $K_{13}[Eu(\alpha\text{-}SiW_{11}O_{39})_2]$ (τ = 2.440 ms) and $Na_{0.5}Cs_{4.5}[Eu(\alpha\text{-}SiW_{11}O_{39})(H_2O)_2]\cdot 23H_2O$ (τ = 0.39 ms),[27] the decay time for **9** is shorter. This phenomenon can be ascribed to the presence of inner-sphere water molecules and the radiationless deactivation of the $^5D_0$ state by coordinated water molecules.[28] Close inspection to the microstructure of **9** will show that there are eight water coordination molecules bonded to the Eu^{III} ion, however, the Eu^{III} cation is coordinated by two water ligands in $Na_{0.5}Cs_{4.5}[Eu(\alpha\text{-}SiW_{11}O_{39})(H_2O)_2]\cdot 23H_2O$ and the Eu^{3+} cation is combined with eight lacunary oxygen atoms from two monovacant $[\alpha\text{-}SiW_{11}O_{39}]^{8-}$ fragments in $K_{13}[Eu(\alpha\text{-}SiW_{11}O_{39})_2]$. Hence, there is no doubt about the shorter luminescence lifetime of **9**.

The solid-state emission spectrum of **11** under excitation at 379 nm displays four obvious emission peaks at 509, 549, 590 and 625 nm, respectively (Fig. 6d). The three typical emission peaks at 549, 590 and 625 nm are respectively attributed to the $^5D_4 \rightarrow {}^7F_5$, $^5D_4 \rightarrow {}^7F_4$ and $^5D_4 \rightarrow {}^7F_3$ transitions of the Tb^{III} cation, which are consistent with the previous results.[29] To clarify the broad and strong emission band centered at 509 nm, the PL emission behavior of the precursor $K_{14}[As_2W_{19}O_{67}(H_2O)]$ has been studied. Upon excitation at 379 nm, the precursor $K_{14}[As_2W_{19}O_{67}(H_2O)]$ exhibits a strong emission band at 509 nm (Fig. 6e), which is induced by the $^3T_{1u} \rightarrow {}^1A_{1g}$ transitions derived from the O → W LMCT transitions of ATs.[22e,30] Comparing the PL spectrum of **11** with that of $K_{14}[As_2W_{19}O_{67}(H_2O)]$, evidently, the broad and strong emission band centered at 509 nm in **11** can be assigned to the $^3T_{1u} \rightarrow {}^1A_{1g}$ transitions from the O → W LMCT transitions of the AT fragments. In addition, the excitation spectrum of **11** was also monitored under excitation at 379 nm and the more intense emission at 549 nm ($^5D_4 \rightarrow {}^7F_5$) of the Tb^{III} ion (Fig. 6f), in which the broad excitation band results from the $^7F_5 \rightarrow {}^5D_3$ transition (379 nm) of the Tb^{III} intra-$4f^8$ ion.[23a,b] To further determine the lifetime, the luminescence decay curve of **11** was also carried out (Fig. 6g). However, the decay curve of **11** can't be fitted to a single exponential function, but a double exponential function $I = A_1\exp(-t/\tau_1) + A_2\exp(-t/\tau_2)$ (where τ_1 and τ_2 are the fast and slow components of the luminescence lifetimes and A_1 and A_2 are the pre-exponential factors) affording the luminescence lifetimes τ_1 and τ_2 as 1.69 μs (9.20%) and 12.74 μs (90.80%), respectively. Since there is one crystallographically independent Tb^{III} ion in the structure of **11**, it is a very slight possibility that **11** has two different lifetimes for the Tb^{III} center. To further probe into the origin of two lifetimes, the luminescence decay curve of the precursor $K_{14}[As_2W_{19}O_{67}(H_2O)]$ was also performed (Fig. 6h), which is

also fitted to a double exponential function with τ_1 and τ_2 of 0.87 μs (24.83%) and 8.83 μs (75.17%), respectively. From this result it can be concluded that the intramolecular transfer of the O → W LMCT energy to the Tb^{III} center has indeed occurred during the course of the emission process of **11**, leading to the appearance of two lifetimes of **11**. This observation further consolidates that the emission behavior of **11** principally stems from the combined action of O → W LMCT transitions and the characteristic $^5D_4 \rightarrow {}^7F_J$ (J = 5–3) transitions of the Tb^{III} cation. Similar intramolecular transfer phenomena from POMs to Tb^{III} ions have been encountered by Yamase and Boskovic.[31,29a] In contrast, comparing the emission spectrum and the luminescence decay curve of **11** with those of the precursor $K_{14}[As_2W_{19}O_{67}(H_2O)]$, the PL emission of **11** prevailingly originates from the contribution of the characteristic $^5D_0 \rightarrow {}^7F_2$ (J = 4–0) transitions of the Eu^{III} cation.

TG analyses

In order to examine their thermal stability, TG measurements of **1–4** and **6–12** were carried out on crystalline samples in a flowing N_2 atmosphere with a heating rate of 10 °C min^{-1} in the temperature range from 25 to 800 °C. All the compounds display two weight loss steps. The TG curves indicate that the weight-loss processes of all the compounds can be divided into two steps. In the case of **1** (Fig. 7a, 1-La), the first weight loss of 6.20% (calcd 6.70%) is from 25 to 96 °C, which is assigned to the liberation of 21 lattice water molecules. The second weight loss of 8.85% (calcd 8.93%) from 94 to 800 °C corresponds to the removal of 17 coordination water molecules and the sublimation of As_2O_3. For **2** (Fig. 7a, 2-Pr), the first weight loss is 5.10% (calcd 6.70%) from 25 to 76 °C, involving the release of 21 lattice water molecules. The second weight loss of 8.16% (calcd 8.92%) from 76 to 800 °C is attributable to the removal of 17 coordination water molecules and the sublimation of As_2O_3 (As_2O_3 is present from the decomposition of the skeleton of the polyoxoanion).[32] In the case of **3** (Fig. 7a, 3-Nd), the first weight loss of 6.53% is (calcd 6.69%) from 25 to 65 °C, is assigned to the liberation of 21 lattice water molecules. The second weight loss of 9.39% (calcd 8.92%) from 65 to 790 °C corresponds to the removal of 17 coordination water molecules and the sublimation of As_2O_3. For **4** (Fig. 7a, 4-Sm), the first weight loss of 6.67% (calcd 6.68%) between 25 and 94 °C is attributable to the liberation of 21 lattice water molecules. The second weight loss of 8.94% (calcd 8.91%) from 94 to 800 °C corresponds to the removal of 17 coordination water molecules and the sublimation of As_2O_3. In regards to **6** (Fig. 7b, 6-Pr), one weight loss (5.12%) between 25 and 63 °C corresponds to the loss of 20 lattice water molecules (calc. 5.94%). After 63 °C, a gradual weight loss of 13.43% up to 800 °C is observed and assigned to the removal of 24 coordination water molecules, the decomposition of two L-thr ligands and the As_2O_3 escaping (calcd 14.34%). With respect to **7** (Fig. 7b, 7-Nd), the weight loss of 6.82% in the first stage from 25 to 93 °C is involved with the release of 20 lattice water molecules (calcd 5.94%). In the second stage, the weight loss of 15.23% is attributable to the removal of 24 coordination water molecules and two L-thr ligands, and the As_2O_3 escaping (calcd 14.32%). With respect to **8** (Fig. 7b, 8-Sm), the weight loss of 5.31% during the first step from 25 to 97 °C involves the loss of 20 lattice water molecules (calcd 5.93%). The weight loss of 13.85% in the second step from 91 to 800 °C is attributable to the removal of 24 coordination water molecules and two L-thr ligands, and the As_2O_3 escaping (calcd 14.30%). As for **9** (Fig. 7b, 9-Eu), the first weight loss between 25 and 78 °C is 5.15% corresponding to the loss of 20 lattice water molecules (calcd 5.92%). Upon further heating, the second weight loss of 13.63% is attributable to the release of 24 coordination water molecules, two L-thr ligands and As_2O_3 (calcd 14.28%). For **10** (Fig. 7c, 10-Gd), the weight loss of 5.89% during the first step from 25 to 91 °C involves the loss of 20 lattice water molecules (calcd 5.91%). The weight loss of 15.00% in the second step from 91 to 800 °C is attributable to the removal of 24 coordination water molecules and two L-thr ligands, and the As_2O_3 escaping (calcd 14.26%). In terms of **11** (Fig. 7c, 11-Tb), the first-step weight loss of 6.14% occurring from 25 to 106 °C corresponds to the loss of 20 lattice water molecules (calcd 5.91%) while the second-step weight loss of 13.49% occurring from 106 to 800 °C is attributable to the removal of 24 coordination water molecules and two L-thr ligands, and the sublimation of As_2O_3 (calcd 14.25%). In regards to **12** (Fig. 7c, 12-Dy), the first step with weight loss of 5.13% is the loss process of 20 lattice water molecules (calcd 5.9%) up to

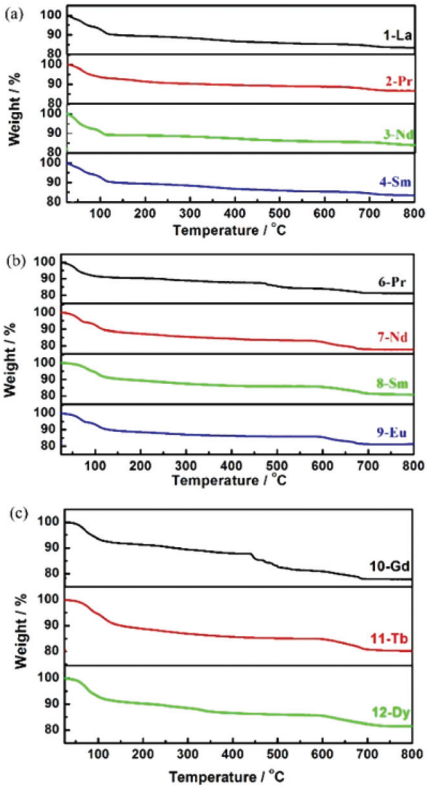

Fig. 7 (a) The TG curves of **1–4**. (b) The TG curves of **6–9**. (c) The TG curves of **10–12**.

81 °C, followed by a weight loss of 13.29% derived from the release of 24 coordination water molecules, two L-thr ligands and As_2O_3 (calcd 14.23%) up to 800 °C.

Conclusions

In conclusion, we have made two types of novel tetra-Fe^{III} substituted sandwich-type ATs with supporting Ln pendants $KNa_2[Ln(H_2O)_7][Fe_4(H_2O)_{10}(B\text{-}\beta\text{-}AsW_9O_{33})_2]\cdot 21H_2O$ [Ln = La^{III} (**1**), Pr^{III} (2), Nd^{III} (**3**), Sm^{III} (**4**)] and $[Ln(H_2O)_8]_2[Fe_4(H_2O)_8(L\text{-thr})_2(B\text{-}\beta\text{-}AsW_9O_{33})_2]\cdot 20\ H_2O$ [Ln = La^{III} (**5**), Pr^{III} (**6**), Nd^{III} (**7**), Sm^{III} (**8**), Eu^{III} (**9**), Gd^{III} (**10**), Tb^{III} (**11**), Dy^{III} (**12**), Er^{III} (**13**)] under 100 °C hydrothermal conditions, which all include classic tetra-Fe^{III} sandwiched $[Fe_4(H_2O)_8(L_2)(B\text{-}\beta\text{-}AsW_9O_{33})_2]^{6-}$ (L = H_2O for **1–4**, L = L-thr for **5–13**) building units with covalent attachments of $[Ln(H_2O)_n]^{3+}$ (n = 7 for **1–4**, n = 8 for **5–13**) cations. Moreover, the degradation of the $[As_2W_{19}O_{67}(H_2O)]^{14-}$ polyoxoanion to the trivacant Keggin AT fragments has occurred during the course of preparing **1–13**, which proves that the bridging {$WO(H_2O)$} group is active and easily escapes from the precursor in the reactions. It is important to emphasize that **1–13** stand for an interface between AT moieties and TM and Ln heterometallic components that are one of the hotspots of a large amount of contemporary research in POM chemistry. Additionally, the luminescence properties of **9** and **11** have been intensively discussed. The results indicate that the PL emission of **9** is mainly derived from the characteristic $^5D_0 \rightarrow {}^7F_2$ (J = 4–0) transitions of the Eu^{III} cations whereas the PL behavior of **11** stems from the common contribution of the $^5D_4 \rightarrow {}^7F_J$ (J = 5–3) transitions of the Tb^{III} ions and the oxygen-to-tungsten charge-transfer transitions of the AT segments. The luminescence decay curve of **9** can be well fitted to a single exponential function with a τ of 9.51 μs whereas the luminescence decay curve of **11** can be fitted to a double exponential function with τ_1 and τ_2 of 1.69 μs (9.20%) and 12.74 μs (90.80%), respectively. Furthermore, the TG curves of **1–4** and **6–12** show two steps of weight loss between 25 and 800 °C. These fruits of our research will guide us to continuously explore and prepare many more novel TM–Ln heterometallic POMs with amino acid ingredients, with the aim of determining some reaction rules between amino acid ligands and TM–Ln heterometallic POM units in this reaction system. The continuous work and unremitting efforts are ongoing.

Acknowledgements

This work was supported by the Natural Science Foundation of China (21101055, 21301049, U1304208), the Natural Science Foundation of Henan Province (122300410106, 102300410093), the Foundation of the State Key Laboratory of Structural Chemistry (20120013), 2014 Special Foundation for Scientific Research Project of Henan University, 2012 Young Backbone Teachers Foundation from Henan Province and the Students Innovative Pilot Plan of Henan University (2013, 2014).

References

1 J. Berzelius, *Pogg. Ann.*, 1826, **6**, 369.
2 (*a*) M. T. Pope, *Heteropoly and Isopoly Oxometalates*, Springer-Verlag, Berlin, Germany, 1983; (*b*) J. J. Borras-Almenar, E. Coronado, A. Müller and M. T. Pope, *Polyoxometalate Molecular Science*, Kluwer Academic Publishers, Dordrecht, The Netherlands, 2003; (*c*) M. AlDamen, J. Clemente-Juan, E. Coronado, C. Martí-Gastaldo and A. Gaita-Ariño, *J. Am. Chem. Soc.*, 2008, **130**, 8847; (*d*) D. L. Long, E. Burkholder and L. Cronin, *Chem. Soc. Rev.*, 2006, **36**, 105; (*e*) G. Absillis and T. N. Parac-Vogt, *Inorg. Chem.*, 2012, **51**, 9902; (*f*) S. T. Zheng, J. Zhang, J. M. Clemente-Juan, D. Q. Yuan and G. Y. Yang, *Angew. Chem., Int. Ed.*, 2009, **48**, 7176.
3 (*a*) U. Kortz, N. K. Al-Kassem, M. G. Savelieff, N. A. Al Kadi and M. Sadakane, *Inorg. Chem.*, 2001, **40**, 4742; (*b*) K. Fukaya and T. Yamase, *Angew. Chem., Int. Ed.*, 2003, **42**, 654; (*c*) B. Godin, Y. Chen, J. Vaissermann, L. Ruhlmann, M. Verdaguer and P. Gouzerh, *Angew. Chem., Int. Ed.*, 2005, **44**, 3072; (*d*) S. S. Mal and U. Kortz, *Angew. Chem., Int. Ed.*, 2005, **44**, 3777; (*e*) B. S. Bassil, M. Ibrahim, R. Al-Oweini, M. Asano, Z. Wang, J. van Tol, N. S. Dalal, K. Y. Choi, R. N. Biboum, B. Keita, L. Nadjo and U. Kortz, *Angew. Chem., Int. Ed.*, 2011, **50**, 5961; (*f*) K. Wassermann, M. H. Dickman and M. T. Pope, *Angew. Chem., Int. Ed. Engl.*, 1997, **36**, 1445; (*g*) B. S. Bassil, M. H. Dickman, I. Römer, B. von der Kammer and U. Kortz, *Angew. Chem., Int. Ed.*, 2007, **46**, 6192; (*h*) F. Hussian, F. Conrad and G. R. Patzke, *Angew. Chem., Int. Ed.*, 2009, **48**, 9088; (*i*) J. Yan, J. Gao, D.-L. Long, H. N. Miras and L. Cronin, *J. Am. Chem. Soc.*, 2010, **132**, 11410; (*j*) J. Gao, J. Yan, S. Beeg, D.-L. Long and L. Cronin, *J. Am. Chem. Soc.*, 2013, **135**, 1796; (*k*) L. Huang, S.-S. Wang, J.-W. Zhao, L. Cheng and G.-Y. Yang, *J. Am. Chem. Soc.*, 2014, **136**, 7637.
4 (*a*) F. Hussain, U. Kortz and R. J. Clark, *Inorg. Chem.*, 2004, **43**, 3237; (*b*) W. Chen, Y. Li, Y. Wang, E. Wang and Z. Su, *Dalton Trans.*, 2007, 4293; (*c*) K. Wassermann, M. H. Dickman and M. T. Pope, *Angew. Chem., Int. Ed. Engl.*, 1997, **36**, 1445; (*d*) J. W. Zhao, D. Y. Shi, L. J. Chen, X. M. Cai, Z. Q. Wang, P. T. Ma, J. P. Wang and J. Y. Niu, *CrystEngComm*, 2012, **14**, 2797.
5 (*a*) F. Hussain, M. Reicke and U. Kortz, *Eur. J. Inorg. Chem.*, 2004, 2733; (*b*) Z. Zhou, D. Zhang, L. Yang, P. Ma, Y. Si, U. Kortz, J. Niu and J. Wang, *Chem. Commun.*, 2013, **49**, 5189.
6 (*a*) C. Tourné, A. Revel, G. Tourné and M. Vendrell, *C. R. Hebd. Seances Acad. Sci., Ser. C*, 1973, **277**, 643; (*b*) U. Kortz, M. G. Savelieff, B. S. Baassil and M. H. Dickman, *Angew. Chem., Int. Ed.*, 2001, **40**, 3384; (*c*) L. H. Bi, U. Kortz, B. Keita, L. Nadjio and L. Daniel, *Eur. J. Inorg. Chem.*, 2005, 3034; (*d*) F. Hussain,

B. S. Baassil, U. Kortz, O. A. Kholdeeva, M. N. Timofeeva, P. D. Oliveira, B. Keita and L. Nadjo, *Chem. – Eur. J.*, 2007, **13**, 4733; (*e*) S. Chang, Y. F. Qi, E. B. Wang, Y. G. Li and H. Jin, *J. Cluster Sci.*, 2007, **18**, 781; (*f*) S. Chang, Y. F. Qi, E. B. Wang, L. Xu, C. Qin, X. L. Wang and H. Jin, *J. Mol. Struct.*, 2008, **875**, 462; (*g*) A. H. Ismail, B. S. Bassil, I. Römer, N. C. Redeker and U. Kortz, *Z. Naturforsch., B: Chem. Sci.*, 2010, **65**, 383; (*h*) C. Ritchie and C. Boskovic, *Cryst. Growth Des.*, 2010, **10**, 488; (*i*) C. Ritchie, M. Speldrich, R. W. Gable, L. Sorace, P. Kögerler and C. Boskovic, *Inorg. Chem.*, 2011, **50**, 7004; (*j*) C. Ritchie, E. G. Moore, M. Speldrich, P. Kögerler and C. Boskovic, *Angew. Chem., Int. Ed.*, 2010, **49**, 7702; (*k*) C. Ritchie, V. Baslon, E. G. Moore, C. Reber and C. Boskovic, *Inorg. Chem.*, 2012, **51**, 1142; (*l*) Q. X. Han, X. P. Sun, J. Li, P. T. Ma and J. Y. Niu, *Inorg. Chem.*, 2012, **53**, 2006.

7 (*a*) S. Reinoso, *Dalton Trans.*, 2011, **40**, 6610; (*b*) Y. Z. Li, J. Luo, L. J. Chen and J. W. Zhao, *RSC Adv.*, 2014, **4**, 50679.

8 (*a*) J. Cao, S. Liu, R. Cao, L. Xie, Y. Ren, C. Gao and L. Xu, *Dalton Trans.*, 2008, 115; (*b*) S. Yao, Z. Zhang, Y. Li, Y. Lu, E. Wang and Z. Su, *Cryst. Growth Des.*, 2010, **10**, 135; (*c*) A. H. Ismail, B. S. Bassil, G. H. Yassin, B. Keita and U. Kortz, *Chem. – Eur. J.*, 2012, **18**, 6163; (*d*) H.-H. Wu, S. Yao, Z.-M. Zhang, Y.-G. Li, Y. Song, Z.-J. Liu, X.-B. Han and E.-B. Wang, *Dalton Trans.*, 2013, **42**, 342; (*e*) Y.-W. Li, Y.-G. Li, Y.-H. Wang, X.-J. Feng, Y. Lu and E.-B. Wang, *Inorg. Chem.*, 2009, **48**, 6452; (*f*) B. Nohra, P. Mialane, A. Dolbecq, E. Rivière, J. Marrot and F. Sécheresse, *Chem. Commun.*, 2009, 2703; (*g*) J. Niu, S. Zhang, H. Chen, J. Zhao, P. Ma and J. Wang, *Cryst. Growth Des.*, 2011, **11**, 3769; (*h*) Z.-M. Zhang, Y.-G. Li, S. Yao and E.-B. Wang, *Dalton Trans.*, 2011, **40**, 6475; (*i*) S. Zhang, J. Zhao, P. Ma, J. Niu and J. Wang, *Chem. – Asian J.*, 2012, **7**, 966; (*j*) S. Zhang, J. Zhao, P. Ma, H. Chen, J. Niu and J. Wang, *Cryst. Growth Des.*, 2012, **12**, 1263; (*k*) X. Fang, M. Speldrich, H. Schilder, R. Cao, K. P. O'Halloran, C. L. Hill and P. Kögerler, *Chem. Commun.*, 2010, **46**, 2760; (*l*) X. Fang and P. Kögerler, *Angew. Chem., Int. Ed.*, 2008, **47**, 8123; (*m*) S. Reinoso, M. Gimónez-Marqués, J. R. Galán-Mascarós, P. Vitoria and J. M. Gutiérrez-Zorrilla, *Angew. Chem., Int. Ed.*, 2010, **49**, 8384; (*n*) W. Chen, Y. Li, Y. Wang and E. Wang, *Eur. J. Inorg. Chem.*, 2007, 2216; (*o*) S. Reinoso and J. R. Galán-Mas carós, *Inorg. Chem.*, 2010, **49**, 377; (*p*) J.-D. Compain, P. Mialane, A. Dolbecq, I. M. Mbomekallé, J. Marrot, F. Sécheresse, C. Duboc and E. Rivière, *Inorg. Chem.*, 2010, **49**, 2851; (*q*) S. Reinoso, J. R. Galán-Mas carós and L. Lezama, *Inorg. Chem.*, 2011, **50**, 9587; (*r*) J.-W. Zhao, Y.-Z. Li, F. Ji, J. Yuan, L.-J. Chen and G.-Y. Yang, *Dalton Trans.*, 2014, **43**, 5694; (*s*) Y.-Y. Li, J.-W. Zhao, Q. Wei, B.-F. Yang, H. He and G.-Y. Yang, *Chem. – Asian J.*, 2014, **9**, 858; (*t*) J. Wang, J.-W. Zhao, H.-Y. Zhao, B.-F. Yang, H. He and G.-Y. Yang, *CrystEngComm*, 2014, **16**, 252; (*u*) J. W. Zhao, D. Y. Shi, L. J. Chen, Y. Z. Li, P. T. Ma, J. P. Wang and J. Y. Niu, *Dalton Trans.*, 2012, **41**, 10740.

9 (*a*) G. Xue, B. Liu, H. Hu, J. Yang, J. Wang and F. Fu, *J. Mol. Struct.*, 2004, **690**, 95; (*b*) A. Merca, A. Müller, J. van Slageren, M. Läge and B. Krebs, *J. Cluster Sci.*, 2007, **18**, 711; (*c*) W. L. Chen, Y. G. Li, Y. H. Wang, E. B. Wang and Z. M. Zhang, *Dalton Trans.*, 2008, 865; (*d*) D. Y. Shi, J. W. Zhao, L. J. Chen, P. T. Ma, J. P. Wang and J. Y. Niu, *CrystEngComm*, 2012, **14**, 3108.

10 F. Zhang, X. Ma, J. Zhang and L. J. Chen, *Chem. Res.*, 2014, **25**(3), 2.

11 (*a*) G. M. Sheldrick, *SHELXS 97, Program for Crystal Structure Solution*, University of Göttingen, Göttingen, Germany, 1997; (*b*) G. M. Sheldrick, *SHELXL 97, Program for Crystal Structure Refinement*, University of Göttingen, Germany, 1997.

12 (*a*) S. Sankar Mal and U. Kortz, *Angew. Chem., Int. Ed.*, 2005, **44**, 377; (*b*) R. Al-Oweini, B. S. Bassil, J. Friedl, V. Kottisch, M. Ibrahim, M. Asano, B. Keita, G. Novitchi, Y. Lan, A. Powell, U. Stimming and U. Kortz, *Inorg. Chem.*, 2014, **53**, 5663; (*c*) R. E. Marsh, *Acta Crystallogr., Sect. B: Struct. Sci.*, 1999, **55**, 931; (*d*) J. W. Zhao, J. Cao, Y. Z. Li, J. Zhang and L. J. Chen, *Cryst. Growth Des.*, 2014, **14**, 6217; (*e*) Y. Y. Li, J. W. Zhao, Q. Wei, B. F. Yang, H. He and G. Y. Yang, *Chem. – Asian J.*, 2014, **9**, 858.

13 (*a*) U. Kortz, M. G. Savelieff, B. S. Bassil, B. Keita and L. Nadjo, *Inorg. Chem.*, 2002, **41**, 783; (*b*) T. McGlone, L. Vila-Nadal, H. N. Miras, D. L. Long, J. M. Poblet and L. Cronin, *Dalton Trans.*, 2010, **39**, 11599; (*c*) M. A. Pilette, S. Floquet, J. Marrot, F. Secheresse and E. Cadot, *Eur. J. Inorg. Chem.*, 2013, 1726; (*d*) A. H. Ismail, B. S. Bassil, I. Römer and U. Z. Kortz, *Anorg. Allg. Chem.*, 2013, **639**, 2510.

14 (*a*) A. Rabenau, *Angew. Chem., Int. Ed. Engl.*, 1985, **24**, 1026; (*b*) P. J. Hagrman, D. Hagrman and J. Zubietua, *Angew. Chem., Int. Ed.*, 1999, **38**, 2638; (*c*) J. W. Zhao, H. P. Jia, J. Zhang, S. T. Zheng and G. Y. Yang, *Chem. – Eur. J.*, 2007, **13**, 10030; (*d*) J. W. Zhao, J. L. Zhang, Y. Z. Li, J. Cao and L. J. Chen, *Cryst. Growth Des.*, 2014, **14**, 1467; (*e*) B. Nohra, P. Mialane, A. Dolbecq, E. Rivière, J. Marrot and F. Sécheresse, *Chem. Commun.*, 2009, 2703.

15 (*a*) M. Bösing, I. Loose, H. Pohlmann and B. Krebs, *Chem. – Eur. J.*, 1997, **3**, 1232; (*b*) U. Kortz, M. G. Savelieff, B. S. Bassil, B. Keita and L. Nadjo, *Inorg. Chem.*, 2002, **41**, 783.

16 S. Li, Y. Wang, P. Ma, J. Wang and J. Niu, *CrystEngComm*, 2014, **16**, 10746.

17 J. Y. Niu, K. H. Wang, H. N. Chen, J. W. Zhao, P. T. Ma, J. Y. Wang, M. X. Li, Y. Bai and D. B. Dang, *Cryst. Growth Des.*, 2009, **9**, 4362.

18 G. Urbain, *C. R. Acad. Sci. Paris*, 1906, **142**, 205.

19 (*a*) E. Soini and I. Hemmilä, *Clin. Chem.*, 1979, **25**, 353; (*b*) I. Hemmilä, T. Ståhlberg and P. Mottram, *Bioanalytical Applications of Labelling Technologies*, Wallac Oy, Turku, Finland, 2nd edn, 1995.

20 (*a*) L. Armelao, S. Quici, F. Barigelletti, G. Accorsi, G. Bottaro, M. Cavazzini and E. Tondello, *Coord. Chem. Rev.*, 2010, **254**, 487; (*b*) B. A. Hess, A. Kedziorski, L. Smentek and D. J. Bornhop, *J. Phys. Chem. A*, 2008, **112**, 2397; (*c*) J.-C. G. Bünzli, A.-S. Chauvin, C. D. B. Vandevyver, B. Song and S. Comby, *Ann. N. Y. Acad. Sci.*, 2008, **1130**, 97.

21 (*a*) G. J. Sopasis, M. Orfanoudaki, P. Zarmpas, A. Philippidis, M. Siczek, T. Lis, J. R. O'Brien and C. J. Milios, *Inorg. Chem.*, 2012, **51**, 1170; (*b*) S. V. Eliseevaa and J.-C. G. Bünzli, *Chem. Soc. Rev.*, 2010, **39**, 189.

22 (*a*) S. L. Cai, S. R. Zheng, Z. Z. Wen, J. Fan and W. G. Zhang, *Cryst. Growth Des.*, 2012, **12**, 5737; (*b*) R. W. Ricci and K. B. Kilichowski, *J. Phys. Chem.*, 1974, **78**, 1953; (*c*) R. M. Supkowski, J. P. Bolender, W. D. Smith, L. E. L. Reynolds and W. D. Horrocks, *Coord. Chem. Rev.*, 1999, **307**, 185; (*d*) T. Yamase, *Chem. Rev.*, 1998, **98**, 307; (*e*) T. Yamase, T. Kobayashi, M. Sugeta and H. Naruke, *J. Phys. Chem. A*, 1997, **101**, 5046; (*f*) T. Ozeki and T. Yamase, *J. Alloys Compd.*, 1993, **192**, 28.

23 (*a*) X. Li, H.-L. Sun, X.-S. Wu, X. Qiu and M. Du, *Inorg. Chem.*, 2010, **49**, 1865; (*b*) P. I. Girginova, F. A. A. Paz, P. C. R. Soares-Santos, R. A. SáFerreira, L. D. Carlos, V. S. Amaral, J. Klinowski, H. I. S. Nogueira and T. Trindade, *Eur. J. Inorg. Chem.*, 2007, 4238; (*c*) J. W. Zhao, J. Luo, L. J. Chen, J. Yuan, H. Y. Li, P. T. Ma, J. P. Wang and J. Y. Niu, *CrystEngComm*, 2012, **14**, 7981; (*d*) R. Gupta, M. K. Saini and F. Hussain, *Eur. J. Inorg. Chem.*, 2014, 6031; (*e*) C. C. Li, S. X. Liu, S. J. Li, Y. Yang, H. Y. Jin and F. J. Ma, *Eur. J. Inorg. Chem.*, 2012, 3229; (*f*) J. W. Zhao, D. Y. Shi, L. J. Chen, Y. Z. Li, P. T. Ma, J. Y. Wang and J. Y. Niu, *Dalton Trans.*, 2012, **41**, 10740.

24 Q. H. Xu, L. S. Li, X. S. Liu and R. R. Xu, *Chem. Mater.*, 2002, **14**, 549.

25 (*a*) A. F. Kirby and F. S. Richardson, *J. Phys. Chem.*, 1983, **87**, 2544; (*b*) J. W. Stouwdam and F. C. J. M. van Veggel, *Nano Lett.*, 2002, **2**, 733; (*c*) Y. Su, L. Li and G. Li, *Chem. Mater.*, 2008, **20**, 6060.

26 (*a*) H. He, G. J. Cao, S. T. Zheng and G. Y. Yang, *J. Am. Chem. Soc.*, 2009, **131**, 15588; (*b*) X. L. Wang, Y. Q. Guo, Y. G. Li, E. B. Wang, C. W. Hu and N. H. Hu, *Inorg. Chem.*, 2003, **42**, 4135; (*c*) T. Yamase, T. Kobayashi, M. Sugeta and H. Naruke, *J. Phys. Chem. A*, 1997, **101**, 5046; (*d*) X. F. Li, T. F. Liu, Q. P. Lin and R. Cao, *Cryst. Growth Des.*, 2010, **10**, 608; (*e*) T. Zhang, C. Spitz, M. Antonietti and C. F. J. Faul, *Chem. – Eur. J.*, 2005, **11**, 1001.

27 P. Mialane, L. Lisnard, A. Mallard, J. Marrot, E. Antic-Fidancev, P. Aschehoug, D. Vivien and F. Sécheresse, *Inorg. Chem.*, 2003, **42**, 2102.

28 A. Beeby, I. M. Clarkson, R. S. Dickins, S. Faulkner, D. Parker, L. Royle, A. S. deSousa, J. A. G. Williams and M. Woods, *J. Chem. Soc., Perkin Trans. 2*, 1999, 493.

29 (*a*) C. Ritchie, E. G. Moore, M. Speldrich, P. Kögerler and C. Boskovic, *Angew. Chem., Int. Ed.*, 2010, **49**, 7702; (*b*) K. Binnemans, *Chem. Rev.*, 2009, **109**, 4283.

30 (*a*) T. Ito, H. Yashiro and T. Yamase, *Langmuir*, 2006, **22**, 2806; (*b*) L. J. Chen, D. Y. Shi, J. W. Zhao, Y. L. Wang, P. T. Ma, J. P. Wang and J. Y. Niu, *Cryst. Growth Des.*, 2011, **11**, 1913.

31 T. Yamase and H. Naruke, *J. Phys. Chem. B*, 1999, **103**, 8850.

32 Q. X. Han, P. T. Ma, J. W. Zhao, Z. L. Wang, W. H. Yang, P. H. Guo, J. P. Wang and J. Y. Niu, *Cryst. Growth Des.*, 2011, **2**, 436.